Array PPP-RTK: A High Precision Pose Estimation Method for Outdoor Scenarios

Xiangdong An, Andrea Bellés, Filippo Rizzi, Lukas Hösch, Christoph Lass, Daniel Medina

***Abstract*—Advanced driver-assistance system (ADAS) and high levels of autonomy for vehicular applications require reliable and high precision pose information for their functioning. Pose estimation comprises solving the localization and orientation problems for a rigid body in a three-dimensional space. In outdoor scenarios, the fusion of Global Navigation Satellite Systems (GNSS) and inertial data in high-end receivers constitutes the baseline for ground truth localization solutions, such as Real-Time Kinematic (RTK) or Precise Point Positioning (PPP). These techniques present two main disadvantages, namely the inability to provide *absolute* orientation information and the lack of observations redundancy in urban scenarios. This paper presents Array PPP-RTK, a recursive three-dimensional pose estimation technique which fuses inertial and multi-antenna GNSS measurements to provide centimeters and sub-degree precision for positioning and attitude estimates, respectively. The core filter is based on adapting the well-known Extended Kalman Filter (EKF), such that it deals with parameters belonging to the SO(3) and GNSS integer ambiguity groups. The Array PPP-RTK observational model is also derived, based on the combination of carrier phase measurements over multiple antennas along with State Space Representation (SSR) GNSS corrections. The performance assessment is based on the real data collected on an inland waterway scenario. The results demonstrate that a high precision solution is available 99.5% of the time, with a horizontal precision of around 6 cm and heading precision of 0.9 degrees. Despite the satellite occlusion after bridge passing, it is shown that Array PPP-RTK recovers high accurate estimates in less than ten seconds.**

***Index Terms*—Pose Estimation; Precise Positioning; Extended Kalman Filtering; GNSS Multi-Antenna; GNSS Inertial Fusion.**

I. Introduction

AUTONOMOUS driving highly depends on navigation systems which tell autonomous vehicles where they are and what the orientations are. To enhance the safety, availability and reliability of Intelligent Transport Systems (ITS), there is an increasing demand for navigation systems to provide continuous and precise position and attitude information. This information is essential and regularly determined by the fusion of Global Navigation Satellite System (GNSS) and Inertial Measurement Units (IMU).

GNSS constitutes the main information supplier for geo-referenced navigation with an all-weather, all-time availability, and a minimal installation and maintenance cost. GNSS code-based localization methods realized instantaneous positioning at meter-level accuracy in open sky conditions. Unfortunately, this precision is insufficient for a plethora of applications requiring decimeter- to centimeter-level precision, e.g. Lane-awareness for automobiles, docking approaches for unmanned vessels or the operation of autonomous drones and robots [1]. Instead, the use of GNSS *carrier phase* observations and correction data is integrated along with inertial measurements to reach precise positioning. Real Time Kinematic (RTK) and Precise Point Positioning (PPP) are the most well-known techniques applied for achieving sub-decimeter positioning. Thus, one finds how geodetic receivers combining RTK and IMU have been widely used in the literatures and serve as positioning baseline in visual odometry benchmarks [2]–[6]. Nevertheless, compared with the relative positioning mode employed in RTK, the absolute positioning of PPP-RTK is a more promising positioning method [7], [8]. Therefore, this paper is motivated to apply tight integration of *Array PPP-RTK* and IMU.

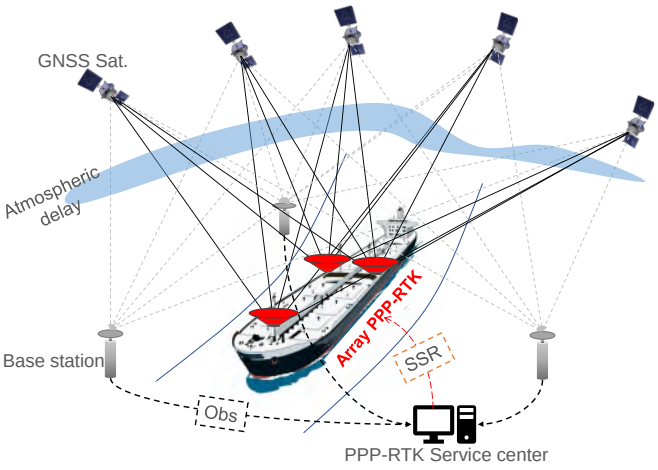

Fig. 1. Array PPP-RTK: a pose estimation technique based on the integration of inertial data, GNSS code and carrier phase measurements from multiple antennas, and the low-bandwidth SSR correction data stream.

Array PPP-RTK is an idea originally from the concept of Array-aided PPP (A-PPP) proposed by Teunissen [9]. It requires a setup of GNSS multiple antennas and a State Space Representation (SSR) correction data stream. Having multiple (an array of) antennas whose relative positions shall be accurately surveyed within the vehicle, brings a twofold benefit: a) it provides *direct* or global orientation information; b) increased GNSS redundancy, which serves to minimize the convergence time and increases the resilience against signal reflection effects. From a methodological perspective, integration

The authors are with the Institute of Communications and Navigation, German Aerospace Center, Neustrelitz 17235, Germany.
(e-mail: xiangdong.ann@gmail.com)

This work was partly funded by the Digital-SOW and Autonom-SOW II projects granted by the German Federal Ministry for Digital and Transport (45DTWV002B and VB18F1025B). It was also partially funded by the European Commission in the IW-Net project (grant number: 861377).

of Array PPP-RTK and IMU is a recursive Bayesian estimator which adapts the Extended Kalman Filter (EKF) to deal with unknown parameters that *live* in the spaces of real numbers (i.e., positioning, velocity, inertial biases, etc.), integer numbers (i.e., for the GNSS carrier phase ambiguities), and the SO(3) manifold (i.e., for the orientation). For handling the geometrical constraints of SO(3), we leverage on Lie Theory and use the Error State form of the EKF, for which the state to be estimated belongs to a manifold and its perturbations *live* in the tangent space of that manifold. Then, for the estimation of the integer parameters we follow the three-step decomposition [10] (float, integer ambiguity, and fixed estimation), and the navigation solution enables sub-dm, sub-degree pose precision [11]–[13]. The contributions of this article mainly include:

1) An Array PPP-RTK observational model based on SSR corrections for simultaneously positioning and attitude determination is derived.
2) The attitude is represented as a quaternion rather than a rotation matrix, which is a minimized representation of the attitude and suitable for integration with IMU measurements.
3) A unified mathematical model is presented to achieve tight integration between Array PPP-RTK and IMU based on EKF.

The rest of the manuscript is organized as follows. Section II presents the related work on precise positioning and attitude determination. Section III describes some preliminary concepts needed for Array PPP-RTK. Then, Section IV offers our contribution on Array PPP-RTK processing and its estimation. Sections V and VI describe the experimental setup and analysis of the results, respectively. Finally, Section VII draws the conclusions and the outlook for this work.

II. Related Work

Precise positioning helps to increase vehicles' autonomy levels, and enhance their safety and competitiveness against conventional transportation. Real-time array calibration (RAC) is a technology that improves the localization of an array of antennas based on real-time error correction [14], [15]. It uses the geometric information of the multiple antennas to narrow and eliminate common errors, and improve the positioning precision. Compared with RAC, Enhanced RAC (ERAC) brings a better error correction by mining more key information [16]. More geometric information is used when correcting vertex measurements, which is beneficial to position estimation. Both RAC and ERAC utilize GNSS code measurements achieving positioning precision at sub-meters to meters level. However, the safety critical-automated driving requires a 20 cm positioning accuracy in horizontal [17]. Thus, GNSS positioning techniques those using code measurements no longer meet the stringent navigational requirements for prospective ITS applications, and it is indispensable to apply centimeter-level positioning methods based on carrier phase measurements, such as RTK [18] and PPP [19].

PPP and RTK are distinguished upon the type of correction data used and the combination of observations. RTK is a differential positioning technique, and the target's position is estimated with respect to a geo-referenced base station. The uncertainty budget for RTK is low and the integer ambiguities can the estimated nearly instantaneously while providing position with centimeter-accuracy [20], [21]. However, the positioning performance rapidly decays as the distance between vehicle and base station grows, and the data stream for the RTK-related corrections requires a broadband and low-latency communication channel. Unlike RTK, PPP is an absolute positioning based on precise satellite orbits and clock products, and uses only the observations from one receiver to calculate its precise position. However, PPP cannot mitigate carrier-phase biases nor reduce the atmospheric delays and, thus, it requires long convergence time until sub-decimeter precise positioning is achieved (ranging from a few minutes to half hour in dynamic scenarios) [22]–[25].

The hybridization of PPP and RTK denoted as PPP-RTK combines the conventional PPP with regional corrections and integer ambiguity resolution to provide quasi-instantaneous centimeter-accurate positioning [7], [26]. In other words, PPP-RTK is based on precise satellite orbit, clock, signal biases, and optional atmospheric products. These products are generated from a GNSS network of stations, encoded as Space State Representation (SSR) information, and broadcasted to users, as illustrated in Fig. 1. Compared with RTK, PPP-RTK has the advantages of saving bandwidth, covering a wide area, and serving unlimited users [7], which better meets the requirements of autonomous driving. Although PPP-RTK achieves instant ambiguity resolution and rapid convergence within 30 seconds by utilizing the state-of-the-art SSR corrections and provides continuous positioning information in an open-sky area, it faces challenges in confined scenarios such as passing through bridges, canyons or urban areas [27]. IMU is an independent sensor providing precise navigation information for a short time when GNSS is unavailable [28]. Tightly coupled PPP-RTK and IMU not only enhanced the solution availability, but also achieved precise positioning at a centimeter to decimeter level within 20 seconds [29], [30]. Therefore, the complementary use of GNSS and IMU will definitely enhance the capability of continuous positioning especially for the applications of transportation.

In addition to positioning, the pose estimation also involves the orientation. The attitude information is usually obtained by IMU and corrected by GNSS measurements in a tight integration of GNSS and IMU system [31], [32] where the IMU requires an initial alignment, leading to the problem that the vehicle needs to stay stationary when aligning the IMU [33], [34]. This initial alignment takes several to tens of minutes which varies with the grade of IMU sensors. This problem can be circumvent with the use of multi-antenna systems. An array of GNSS antennas increases the data redundancy, its benefits on calculating satellite phase biases, sensing ionosphere and improving ambiguity resolution have been investigated and proved [35]–[37]. We focus on antenna array aided attitude determination, which was indeed one of the pioneer uses of GNSS in space missions [38]–[40] to determine the orientation of satellites and space probes. GNSS antenna array represents an appealing alternative to magnetometers, gyroscopes or orientation odometry, and provides a

drift-less absolute orientation with a fair compromise in terms of cost, weight, and precision. Thus, the array-aided GNSS attitude problem has been extensively studied.

A precondition of precise attitude determination in a GNSS antenna array system is ambiguity resolution. Based on the Least-squares Ambiguity Decorrelation Adjustment (LAMBDA) method [10], some famous attitude determination models were proposed, such as C-LAMBDA (baseline length Constrained LAMBDA), MC-LAMBDA (Multivariate Constrained LAMBDA), and AC-LAMBDA (Affine Constrained LAMBDA). The C-LAMBDA adds nonlinear baseline length constraints into the process of ambiguity resolution benefiting the search for the correct integer ambiguity vector [41]–[43]. MC-LAMBDA is a further extension based on C-LAMBDA, which makes full use of prior information of the antenna configurations including not only the baseline length but also the relative orientation of the multiple antennas [44]–[47]. Although C-LAMBDA and MC-LAMBDA have an increased success rate in comparison with classical LAMBDA, the rigorous inclusion of the nonlinear constraints into the ambiguity objective function has made the complexity of its integer ambiguity search increase as well. Thus, an AC-LAMBDA was proposed to make a compromise between the unconstrained LAMBDA and its more complex MC-LAMBDA [48]. It decomposed the attitude constraints into linear and quadratic constraints. By disregarding the quadratic constraints and only keeping the linear constraints, it avoided the computational complexity of the MC-LAMBDA through directly using the standard LAMBDA method [49]. However, the linear constraints are only present when the number of baselines is larger than the dimension of their span, which means if we would like to determine the attitude in 3D, we can only get some benefits from the AC-LAMBDA when the number of antennas is greater than three.

Besides the GNSS attitude determination models, the literatures for GNSS high precision pose estimation, i.e., solving simultaneously the localization and attitude for a vehicle, are limited to two techniques: A-PPP, and Joint Positioning and Attitude determination (JPA). A-PPP proposed a unified model to estimate the position and attitude simultaneously [9] in an antenna array system. The attitude was parameterized as a rotation matrix and the ambiguity resolution was realized through solving a novel orthonormality-constrained multivariate (mixed) integer least-squares problem. Finally, it improved the success rate of single-epoch ambiguity resolution [37], [50]–[52]. However, A-PPP is not designed for the tight integration with IMU, because the rotation matrix is not a minimum representation of the attitude. Some trigonometric functions must be employed to get the pitch, roll, and yaw angles of the vehicle. Consequently, the variance-covariance information of the three attitude angles is missing or hard to obtain, making it inconvenient to achieve tight integration with IMU. Instead of PPP, JPA method combines the RTK with attitude information in a multi-antenna system and represents the attitude as a quaternion in the state vector. The position and attitude parameters are simultaneously estimated by an Error-State Kalman Filter (ESKF) [53], [54]. In this work, we extend the theory behind A-PPP and JPA, and contribute Array PPP-RTK aided with IMU. Array PPP-RTK constitutes the most ambitious high precision GNSS navigation technique to date and provides an precise pose estimation with tight integration of IMU in a multi-antenna, multi-sensor system.

III. Preliminaries

A. Coordinate Frames and Transformations

It generally involves three coordinate frames in navigation: *1)* the *body* frame (*b*-frame) whose motion is described; *2)* the geo-referenced frame (*e*-frame) with which the motion is respect to; *3)* the auxiliary *navigation* frame (*n*-frame) for describing the vehicle's movement in an accessible manner. The relationship between different frames is illustrated in Fig. 2.

Let us consider a multi-sensor and multi-antenna platform which includes $N+1$ GNSS antennas and at least one IMU. The *main* and the remaining N *secondary* antennas are referred to with the subscripts m and $s \in (1,\dots,N)$, respectively. The relative positions of the antennas and IMU are as depicted on Fig. 2b. Since the relative positions of antennas are surveyed and accurately known within the body frame. Then the s^{th} baseline vector in n-frame (${}_{\mathfrak{n}}\mathbf{d}_{sm}$) can be formulated as

$$ {}_{n}\mathbf{d}_{s,m} = \mathbf{q} \circ {}_{b}\mathbf{d}_{sm} \circ \mathbf{q}^{-1},\ s \in (1,\dots,N), \tag{1}$$

where $\circ$ is the operator of quaternion multiplication; $\mathbf{q}$ is the unit-quaternion to represent the body-to-navigation rotation which is defined as

$$ \mathbf{q} = \begin{bmatrix} q_w \\ \mathbf{q}_{\mathfrak{u}} \end{bmatrix} = \mathbf{q}\{\mathbf{e}\varphi\} = \begin{bmatrix} \cos(\varphi/2) \\ \mathbf{e}\sin(\varphi/2) \end{bmatrix} \tag{2}$$

with q_w and $\mathbf{q}_{\mathfrak{u}}$ the real and complex parts of quaternion, $\mathbf{e}$ a unit rotation axis and φ a rotation angle from b-frame to n-frame; $\mathbf{q}^{-1}$ is the inverse of $\mathbf{q}$. Our task would be briefly summarized as simultaneously estimating the position of the main antenna, and determining the rotation between the body and navigation frames in an extended Kalman filter.

B. Lie Theory for Kalman Filtering

Consider a generic state estimation vector composed by the vector of unknown $\mathbf{u}$ and the orientation $\mathbf{q}$, such that $\mathbf{x}^\top = [\mathbf{u}^\top, \mathbf{q}^\top]$, where $(\cdot)^\top$ means transpose of a vector/matrix. Then, the error state is described by $\delta\mathbf{x}^\top = [\delta\mathbf{u}^\top, \delta\boldsymbol{\theta}^\top]$. Here, $\delta\boldsymbol{\theta}$ the rotation vector. The Euclidean space for $\delta\boldsymbol{\theta}$ connects to the Lie algebra $\mathbf{e}\varphi \in \mathfrak{s}^3$ (with $\mathbf{e}$ an unit vector of rotation, and φ the rotated angle) with the isomorphism $(\cdot)^\wedge : \mathbb{R}^3 \mapsto \mathfrak{s}^3$. Then, the Lie algebra connects with the 3D unit-sphere $\mathcal{S}^3$ manifold through exponential mapping [55], [56]. The overall procedure is given by

$$ \delta\boldsymbol{\theta} \in \mathbb{R}^3 \xrightarrow{(\cdot)^\wedge} \mathbf{e}\varphi \in \mathfrak{s}^3 \xrightarrow{\exp(\cdot)} \delta\mathbf{q} \in \mathcal{S}^3, \tag{3}$$
$$ (\delta\boldsymbol{\theta})^\wedge : \begin{cases} \mathbf{e} = \frac{\delta\boldsymbol{\theta}}{\|\delta\boldsymbol{\theta}\|^2} \\ \varphi = \|\delta\boldsymbol{\theta}\|^2 \end{cases}, \exp(\mathbf{e}\varphi) : \begin{bmatrix} \cos(\varphi/2) \\ \mathbf{e}\sin(\varphi/2) \end{bmatrix}.$$

Thus, $\mathbf{q}\{\boldsymbol{\theta}\}$ corresponds to the mapping between the Euclidean space and the unit quaternion as in (2). With the Lie

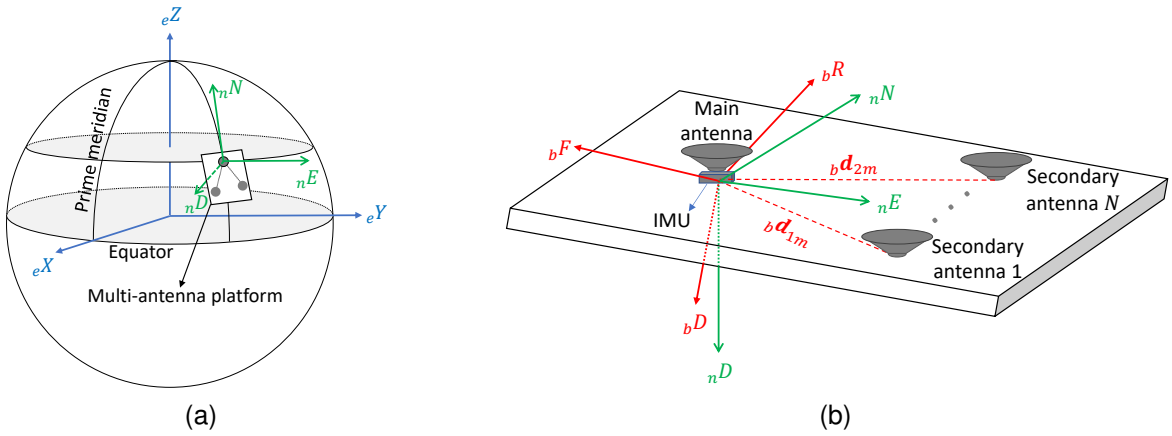

Fig. 2. Relationship between global frame, navigation frame, and body frame. (a) The global frame is a Earth-Centered, Earth-Fixed (ECEF) coordinate frame, indicated as e and its axes are $({}_eX, {}_eY, {}_eZ)$; The navigation frame is also known as a local geodetic coordinate system, denoted as n and the axes $({}_nN, {}_nE, {}_nD)$ means north, east, down. (b) The body frame is illustrated as b and its axes $({}_bF, {}_bR, {}_bD)$ means front, right, down. Both the n-frame and b-frame are referenced to the position of the main antenna and move with the platform.

Theory tools now widely available, the composition of nominal and error state is expressed as

$$\mathbf{x} = \mathbf{x}_0 \oplus \delta\mathbf{x} = \begin{cases} \mathbf{u}_0 & + & \delta\mathbf{u} \\ \mathbf{q}_0 & \circ & \delta\mathbf{q}\{\delta\boldsymbol{\theta}\} \end{cases}, \tag{4}$$

Thus, the ESKF adapts the standard Kalman Filter framework for a chosen non-linear parametrization (here formulated for a generic state vector by (4)) to preserve the unit-norm quaternion constraint [57]–[59].

IV. Array PPP-RTK Processing

Array PPP-RTK is a technique for the recursive estimation of a vehicle's kinematic properties based on the fusion of inertial and GNSS multi-antenna data. From a practical implementation perspective, Array PPP-RTK requires the integration of three main modules under the same platform as shown in Fig. 3:

1) Reference station network. The stations are even distributed in a region and constitute a Continuous Operation Reference Station (CORS) network, which could be a national, continental, and even global network. For example, the German Satellite Positioning Service (SAPOS) collects the GNSS data and transmits it to PPP-RTK service center in real-time.
2) PPP-RTK service center. It receives data from a reference station network, and computes precise orbit and clock corrections with respect to GNSS broadcast ephemeris. Besides, it also generates signal biases enabling users to resolve integer ambiguities. To speed up the convergence time of PPP-RTK, tropospheric and ionospheric model parameters are also estimated, represented as SSR corrections, and broadcasted to PPP-RTK users.
3) Multi-sensor, multi-antenna system. The core of this system is Array PPP-RTK processing engine, which starts from an initialization and sets the initial state vector of the Kalman filter. It then uses the acceleration and angular rate of the IMU as data inputs to predict the position and attitude. Followed by the state update, in this phase the precise satellite orbit, clock, signal biases, tropospheric and ionospheric delays are derived from the SSR products; Based on the IMU predicted state, the error state of position and attitude are simultaneously updated by using GNSS code and phase measurements from the multi-antenna. The updated solutions are then used to correct the state predicted by IMU. In addition, ambiguity resolution is implemented to improve the precision of the state estimation, if ambiguity resolution succeeds then derive the solutions with ambiguities fixed to integers, otherwise keep the ambiguities as float values and proceed to the next epoch.

We will present the mathematical models for Array PPP-RTK processing engine starting from the GNSS observation equations in a multi-antenna platform, followed by the attitude determination based on a quaternion representation, and then the prediction and correction of Kalman filter. Finally, the ambiguity resolution is adopted to improve the performances.

A. GNSS Observation Equation based on SSR Corrections

GNSS observation equations of double-frequency code and phase measurements from satellite i to the main antenna m are written as

$$\begin{cases} P^i_{m,1} = \rho^i_m + c(t_m - dt^{i,P1}) + M^i \cdot T_m + I^i_m \\ \qquad + \epsilon(P^i_{m,1}) \\ P^i_{m,2} = \rho^i_m + c(t_m - dt^{i,P2}) + M^i \cdot T_m + g \cdot I^i_m \\ \qquad + h_{m,2} + \epsilon(P^i_{m,2}) \\ L^i_{m,1} = \rho^i_m + c(t_m - dt^{i,L1}) + M^i \cdot T_m - I^i_m \\ \qquad + \lambda_1 \cdot \widetilde{a}^i_{m,1} + \epsilon(L^i_{m,1}) \\ L^i_{m,2} = \rho^i_m + c(t_m - dt^{i,L2}) + M^i \cdot T_m - g \cdot I^i_m \\ \qquad + \lambda_2 \cdot \widetilde{a}^i_{m,2} + \epsilon(L^i_{m,2}) \\ S^i_{m,T} = M^i \cdot T_m + \epsilon(S^i_{m,T}) \\ S^i_{m,I} = I^i_m + \epsilon(S^i_{m,I}) \end{cases} \tag{5}$$

where

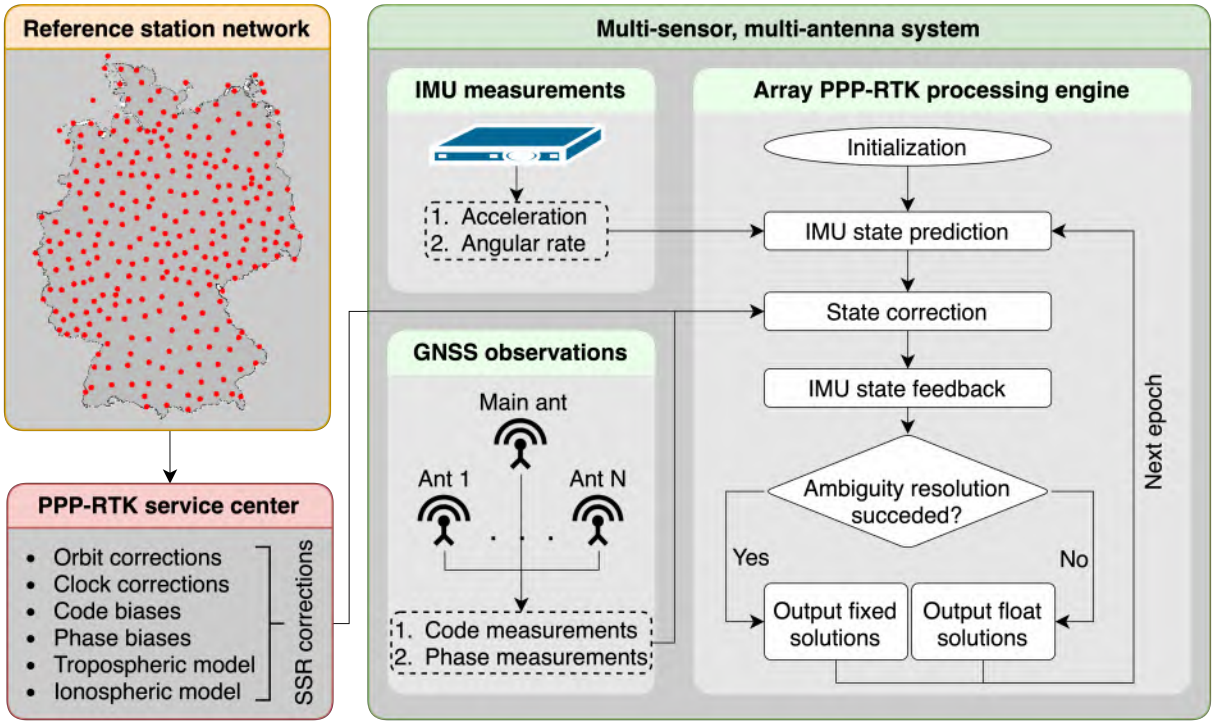

Fig. 3. Flowchart of data acquisition and processing chain, which includes three modules (1) Reference station network, (2) PPP-RTK service center, and (3) Multi-sensor, multi-antenna system.

- $P^i_{m,1}, P^i_{m,2}$ mean the code measurements from a satellite i to the main antenna m at the first and second frequency, respectively;
- $L^i_{m,1}, L^i_{m,2}$ stand for the corresponding phase measurements;
- $\rho^i_m = \sqrt{(X^i - X_m)^2 + (Y^i - Y_m)^2 + (Z^i - Z_m)^2}$ is the geometric distance between the satellite position (X^i, Y^i, Z^i) and antenna position (X_m, Y_m, Z_m);
- c is the speed of light in a vacuum and t_m the receiver clock offset;
- $dt^{i,P1}, dt^{i,P2}, dt^{i,L1}, dt^{i,L2}$ are SSR satellite clock offset plus signal biases for each type of measurements;
- T_m is the zenith tropospheric delay and M^i maps the zenith delay to slant delay [60];
- I^i_m means the slant ionospheric delay, $g = \frac{f_1^2}{f_2^2}$ is the ratio of the ionospheric delay between the first and second frequencies, and f_1, f_2 denote the signal frequencies;
- $h_{m,2}$ is receiver code bias of the second frequency with respect to the first frequency;
- λ_1 and λ_2 denote the signal wavelength;
- $\widetilde{a}$ indicates the float ambiguity, which includes integer ambiguity plus the phase biases of receiver and satellite;
- $S^i_{m,T}$ and $S^i_{m,I}$ are slant tropospheric and ionospheric delays calculated based on SSR atmospheric model;
- ε represents the corresponding noise of measurements.

The linearization of (5) is formulated in a matrix format as

$$\begin{bmatrix} \widetilde{P}^i_{m,1} \\ \widetilde{P}^i_{m,2} \\ \widetilde{L}^i_{m,1} \\ \widetilde{L}^i_{m,2} \\ S^i_{m,T} \\ S^i_{m,I} \end{bmatrix} = \begin{bmatrix} \mathbf{J}^i_m \mathbf{C}^n_e & c & 0 & M^i & 1 & 0 & 0 \\ \mathbf{J}^i_m \mathbf{C}^n_e & c & 1 & M^i & g & 0 & 0 \\ \mathbf{J}^i_m \mathbf{C}^n_e & c & 0 & M^i & -1 & \lambda_1 & 0 \\ \mathbf{J}^i_m \mathbf{C}^n_e & c & 0 & M^i & -g & 0 & \lambda_2 \\ \mathbf{0} & 0 & 0 & M^i & 0 & 0 & 0 \\ \mathbf{0} & 0 & 0 & 0 & 1 & 0 & 0 \end{bmatrix} \begin{bmatrix} \delta \mathbf{p}_m \\ t_m \\ h_{m,2} \\ T_m \\ I^i_m \\ \widetilde{a}^i_{m,1} \\ \widetilde{a}^i_{m,2} \end{bmatrix} \tag{6}$$

in which

$$\begin{cases} \widetilde{P}^i_{m,1} = P^i_{m,1} - \rho^i_m + c \cdot dt^{i,P1} \\ \widetilde{P}^i_{m,2} = P^i_{m,2} - \rho^i_m + c \cdot dt^{i,P2} \\ \widetilde{L}^i_{m,1} = L^i_{m,1} - \rho^i_m + c \cdot dt^{i,L1} \\ \widetilde{L}^i_{m,2} = L^i_{m,2} - \rho^i_m + c \cdot dt^{i,L2} \end{cases} \tag{7}$$

and $\delta \mathbf{p}_m = (\delta N_m, \delta E_m, \delta D_m)$ denoting the position adjustment in n-frame. The Jacobian matrix $\mathbf{J}^i_m$ is calculated by

$$\mathbf{J}^i_m = \left[-\frac{X^i - X_m}{\rho^i_m}, -\frac{Y^i - Y_m}{\rho^i_m}, -\frac{Z^i - Z_m}{\rho^i_m} \right]. \tag{8}$$

The rotation matrix from e-frame to n-frame is represented by $\mathbf{C}^n_e$ and formulated as [61]

$$\mathbf{C}^n_e = \begin{bmatrix} -cos(lon)sin(lat) & -sin(lon) & -cos(lon)cos(lat) \\ -sin(lon)sin(lat) & cos(lon) & -sin(lon)cos(lat) \\ cos(lat) & 0 & -sin(lat) \end{bmatrix} \tag{9}$$

where (lat, lon) are ellipsoidal latitude and longitude of the antenna position. The secondary antenna is mounted quite close to the main antenna, thus similar to (6), the GNSS

observation equation from satellite i to a secondary antenna $s \in (1, \ldots, N)$ is linearized as

$$\begin{bmatrix} \widetilde{P}^i_{s,1} \\ \widetilde{P}^i_{s,2} \\ \widetilde{L}^i_{s,1} \\ \widetilde{L}^i_{s,2} \end{bmatrix} = \begin{bmatrix} \mathbf{J}^i_m \mathbf{C}^n_e & c & 0 & M^i & 1 & 0 & 0 \\ \mathbf{J}^i_m \mathbf{C}^n_e & c & 1 & M^i & g & 0 & 0 \\ \mathbf{J}^i_m \mathbf{C}^n_e & c & 0 & M^i & -1 & \lambda_1 & 0 \\ \mathbf{J}^i_m \mathbf{C}^n_e & c & 0 & M^i & -g & 0 & \lambda_2 \end{bmatrix} \begin{bmatrix} \delta \mathbf{p}_s \\ t_s \\ h_{s,2} \\ T_s \\ I^i_s \\ \widetilde{a}^i_{s,1} \\ \widetilde{a}^i_{s,2} \end{bmatrix}, \tag{10}$$

where $\delta \mathbf{p}_s = (\delta N_s, \delta E_s, \delta D_s)$ denoting the position adjustment for antenna s in n-frame and

$$\begin{cases} \widetilde{P}^i_{s,1} = P^i_{s,1} - \rho^i_m + c \cdot dt^{i,P1} \\ \widetilde{P}^i_{s,2} = P^i_{s,2} - \rho^i_m + c \cdot dt^{i,P2} \\ \widetilde{L}^i_{s,1} = L^i_{s,1} - \rho^i_m + c \cdot dt^{i,L1} \\ \widetilde{L}^i_{s,2} = L^i_{s,2} - \rho^i_m + c \cdot dt^{i,L2} \end{cases}. \tag{11}$$

The double-differenced GNSS code and phase observation equations between satellites (i, j) and antennas (s, m) are expressed as

$$\begin{bmatrix} \widetilde{P}^{ij}_{sm,1} \\ \widetilde{P}^{ij}_{sm,2} \\ \widetilde{L}^{ij}_{sm,1} \\ \widetilde{L}^{ij}_{sm,2} \end{bmatrix} = \begin{bmatrix} \mathbf{J}^{ij}_{sm} \mathbf{C}^n_e & 0 & 0 \\ \mathbf{J}^{ij}_{sm} \mathbf{C}^n_e & 0 & 0 \\ \mathbf{J}^{ij}_{sm} \mathbf{C}^n_e & \lambda_1 & 0 \\ \mathbf{J}^{ij}_{sm} \mathbf{C}^n_e & 0 & \lambda_2 \end{bmatrix} \begin{bmatrix} {}_n\mathbf{d}_{sm} \\ a^{ij}_{sm,1} \\ a^{ij}_{sm,2} \end{bmatrix}, \tag{12}$$

where ${}_n\mathbf{d}_{sm} = \delta \mathbf{p}_s - \delta \mathbf{p}_m$ is the baseline vector between the secondary and main antennas in n-frame, e.g. ${}_n\mathbf{d}_{1m}$ and ${}_n\mathbf{d}_{1m}$ illustrated in Fig. 2b. $\mathbf{J}^{ij}_{sm} = (\mathbf{J}^i_s - \mathbf{J}^j_s) - (\mathbf{J}^i_m - \mathbf{J}^j_m)$. $\widetilde{P}^{ij}_{sm,1}$, $\widetilde{P}^{ij}_{sm,2}$ and $\widetilde{L}^{ij}_{sm,1}$, $\widetilde{L}^{ij}_{sm,2}$ are double-differenced code and phase measurements between two satellites i, j and two stations s, m. $a^{ij}_{sm,1}$ and $a^{ij}_{sm,2}$ indicate the corresponding double-differenced ambiguities at the first and second frequencies. One should note that the receiver clock offset t_s, code bias $h_{s,2}$ are mitigated in the double-differencing operation. Moreover, tropospheric and ionospheric delays are significantly reduced and ignored in (12) due to the fact the distance between the secondary and main antennas is short, i.e. only several meters.

In (6) and (12), the left item of equation is considered as an Observed Minus Computed (OMC) vector, the first and second items at the right side of equation are seen as design matrix and state vector. If we combine the OMC vector, design matrix, and state vector of (6) and (12) in one formula, it can be written as

$$\begin{bmatrix} \mathbf{y}_m \\ \mathbf{y}_{sm} \end{bmatrix} = \begin{bmatrix} \mathbf{H}^{\delta \mathbf{p}}_m & \mathbf{0} & \mathbf{H}^{\mathbf{o}}_m & \mathbf{H}^{\mathbf{a}}_m & \mathbf{0} \\ \mathbf{0} & \mathbf{H}^{\mathbf{d}_{sm}}_{sm} & \mathbf{0} & \mathbf{0} & \mathbf{H}^{\mathbf{a}}_{sm} \end{bmatrix} \begin{bmatrix} \delta \mathbf{p}_m \\ {}_n\mathbf{d}_{sm} \\ \mathbf{o}_m \\ \widetilde{\mathbf{a}}_m \\ \mathbf{a}_{sm} \end{bmatrix} \tag{13}$$

in which $\mathbf{y}_m$ is undifferenced OMC vector for the main antenna; $\mathbf{y}_{sm}$ are double-differenced OMC vectors for the secondary-main antenna pairs $sm, s \in (1, \ldots, N)$. The subscript of $\mathbf{H}$ indicates the design matrix corresponding to main antenna m or a secondary-main antenna pair (sm); Its superscript marks the type of parameters, such as position $\mathbf{p}$, baselines $\mathbf{d}_{sm}$, and ambiguities $\mathbf{a}$; The other parameters for the main antennas, e.g. receiver clock offset, code bias, tropospheric, and ionospheric delays, are denoted as $\mathbf{o}$. Equation (13) is the GNSS observation equation in a multi-antenna platform, and in the next section we are going to talk about how to convert the baseline vectors (${}_n\mathbf{d}_{sm}$) to attitude parameters in the GNSS observational model.

B. Quaternion-Based Attitude Representation

The state vector in (13) does not contain any attitude information. From (1), we know the baseline in n-frame is a function of quaternion:

$${}_n\mathbf{d}_{sm} = f(\mathbf{q}) = \mathbf{q} \circ {}_b\mathbf{d}_{sm} \circ \mathbf{q}^{-1} \tag{14}$$

where ${}_b\mathbf{d}_{sm}$ means the baseline vector in b-frame which is known and precisely pre-measured, $\mathbf{q}$ is a quaternion containing rotation information which is unknown and needs to be determined. The true state of quaternion is decomposed into a nominal state $\mathbf{q}_0$ and error state $\delta \mathbf{q}$ as

$$\mathbf{q} = \mathbf{q}_0 \circ \delta \mathbf{q}. \tag{15}$$

This decomposition could be understood like two consecutive rotations: the initial rotation represented by $\mathbf{q}_0$ with an angle of $\boldsymbol{\theta}$ and an adjustment rotation indicated by $\delta \mathbf{q}$ with an angle of $\delta \boldsymbol{\theta}$. The Jacobian matrix of ${}_n\mathbf{d}_{sm}$ with respect to $\delta \mathbf{q}$ is derived based on the chain rule as

$$\mathbf{J}^{\delta \boldsymbol{\theta}}_{sm} = \frac{\partial f(\mathbf{q})}{\partial \delta \boldsymbol{\theta}} = \frac{\partial (\mathbf{q} \circ {}_b\mathbf{d}_{sm} \circ \mathbf{q}^{-1})}{\partial \mathbf{q}} \frac{\partial \mathbf{q}}{\partial \delta \mathbf{q}} \frac{\partial \delta \mathbf{q}}{\partial \delta \boldsymbol{\theta}}. \tag{16}$$

The detailed derivation of derivatives in (16) can be found in [62], their results are given here without explanation as

$$\begin{aligned} \frac{\partial (\mathbf{q} \circ {}_b\mathbf{d}_{sm} \circ \mathbf{q}^{-1})}{\partial \mathbf{q}} &= 2[q_w \cdot {}_b\mathbf{d}_{sm} - [{}_b\mathbf{d}_{sm} \times] \mathbf{q}_\mathbf{u}, \\ &\mathbf{q}_\mathbf{u}{}^\top \cdot {}_b\mathbf{d}_{sm} \mathbf{I}_3 + \mathbf{q}_\mathbf{u} \cdot {}_b\mathbf{d}_{sm} - {}_b\mathbf{d}_{sm} \mathbf{q}_\mathbf{u}{}^\top - q_w [{}_b\mathbf{d}_{sm} \times]] \end{aligned}, \tag{17}$$

$$\frac{\partial \mathbf{q}}{\partial \delta \mathbf{q}} = \frac{\partial (\mathbf{q}_0 \circ \delta \mathbf{q})}{\partial \delta \mathbf{q}} = q_w \mathbf{I}_4 + \begin{bmatrix} 0 & -\mathbf{q}_\mathbf{u}{}^\top \\ \mathbf{q}_\mathbf{u} & [\mathbf{q}_\mathbf{u} \times] \end{bmatrix}, \tag{18}$$

and

$$\frac{\partial \delta \mathbf{q}}{\partial \delta \boldsymbol{\theta}} = \frac{1}{2} \begin{bmatrix} 0 & 0 & 0 \\ 1 & 0 & 0 \\ 0 & 1 & 0 \\ 0 & 0 & 1 \end{bmatrix}, \tag{19}$$

where $[{}_b\mathbf{d}_{sm} \times]$ and $[\mathbf{q}_\mathbf{u} \times]$ are the skew-symmetric matrix of ${}_b\mathbf{d}_{sm}$ and $\mathbf{q}_\mathbf{u}$. Based on (14), (15) and (16), we get the linearized equations for the secondary-main baseline vector

$${}_n\mathbf{d}_{sm} = \mathbf{q}_0 \circ {}_b\mathbf{d}_{sm} \circ \mathbf{q}_0^{-1} + \mathbf{J}^{\delta \boldsymbol{\theta}}_{sm} \delta \boldsymbol{\theta} \tag{20}$$

Substitute (20) into (13) and derive

$$\begin{bmatrix} \mathbf{y}_m \\ \widetilde{\mathbf{y}}_{sm} \end{bmatrix} = \begin{bmatrix} \mathbf{y}_m \\ \mathbf{y}_{sm} - \mathbf{H}^{\mathbf{d}_{sm}}_{sm} (\mathbf{q}_0 \circ {}_b\mathbf{d}_{sm} \circ \mathbf{q}_0^{-1}) \end{bmatrix} =$$

$$\begin{bmatrix} \mathbf{H}^{\delta \mathbf{p}}_m & \mathbf{0} & \mathbf{H}^{\mathbf{o}}_m & \mathbf{H}^{\mathbf{a}}_m & \mathbf{0} \\ \mathbf{0} & \mathbf{H}^{\delta \boldsymbol{\theta}}_{sm} & \mathbf{0} & \mathbf{0} & \mathbf{H}^{\mathbf{a}}_{sm} \end{bmatrix} \begin{bmatrix} \delta \mathbf{p}_m \\ \delta \boldsymbol{\theta} \\ \mathbf{o}_m \\ \widetilde{\mathbf{a}}_m \\ \mathbf{a}_{sm} \end{bmatrix} \tag{21}$$

with

$$\mathbf{H}_{sm}^{\delta\boldsymbol{\theta}} = \mathbf{H}_{sm}^{\mathbf{d}_{sm}} \mathbf{J}_{sm}^{\delta\boldsymbol{\theta}}. \tag{22}$$

Equation (21) is the mathematical model for Array PPP-RTK in a multi-antenna platform. In the next section, the IMU is fused within this mathematical model and the ESKF is adopted to solve this equation.

C. Error State Kalman Filter

1) State vector: From (21), we can see the state vector includes position, attitude, receiver clock offset, code bias, atmospheric delays, and ambiguities. However, in a multi-sensor platform of GNSS and IMU, the state vector also includes parameters corresponding to IMU, such as velocity, gyroscope and accelerometer biases. To make it clear, we classify the parameters in four groups:

$$\mathbf{x} = \left[\mathbf{x}_{\text{kin}}^\top \ \mathbf{x}_{\text{IMU}}^\top \ \mathbf{x}_{\text{GNSS}}^\top \ \mathbf{x}_{\text{a}}^\top\right]^\top, \tag{23}$$

$$\mathbf{x}_{\text{kin}} = \left[\delta\mathbf{p}^\top \ \delta\mathbf{v}^\top \ \delta\boldsymbol{\theta}^\top\right]^\top, \tag{24}$$

$$\mathbf{x}_{\text{IMU}} = \left[\mathbf{b}_a^\top \ \mathbf{b}_\omega^\top\right]^\top, \tag{25}$$

$$\mathbf{x}_{\text{GNSS}} = \left[\mathbf{t}_m^\top \ T_m \ \mathbf{i}^\top\right]^\top, \tag{26}$$

$$\mathbf{x}_{\text{a}} = \left[\widetilde{\mathbf{a}}_m^\top \ \mathbf{a}_{1m}^\top \ \dots \ \mathbf{a}_{Nm}^\top\right]^\top, \tag{27}$$

where $\mathbf{x}_{\text{kin}}$ means kinematic parameters including error state of position ($\mathbf{p}$), velocity ($\mathbf{v}$), and attitude ($\boldsymbol{\theta}$); $\mathbf{x}_{\text{IMU}}$ indicates the bias parameters of accelerometer ($\mathbf{b}_a$) and gyroscope ($\mathbf{b}_\omega$); $\mathbf{x}_{\text{GNSS}}$ includes the GNSS related parameters, such as receiver clock offset ($\mathbf{t}_m$), tropospheric delay (T_m), Ionospheric delays for satellite-receiver pairs ($\mathbf{i}$); $\mathbf{x}_{\text{a}}$ denotes ambiguities for main antenna ($\mathbf{a}_m$) and double differenced ambiguities for secondary-main antenna pairs ($\mathbf{a}_{1m}, \dots, \mathbf{a}_{Nm}$).

2) Prediction step with IMU: In prediction phase, the mechanization process of Inertial Navigation System (INS) uses IMU outputs to predict the velocity, position, and attitude of the object. The state transition matrices for $\mathbf{x}_{\text{kin}}$ and $\mathbf{x}_{\text{IMU}}$ are derived by the relative state dynamic model of INS [63], [64]:

$$\begin{cases} \delta\dot{\mathbf{p}} = -\boldsymbol{\omega}_{en}^n \times \delta\mathbf{p} + \delta\mathbf{v} \\ \delta\dot{\mathbf{v}} = -(\boldsymbol{\omega}_{en}^n + 2\boldsymbol{\omega}_{ie}^n) \times \delta\mathbf{v} + \mathbf{C}_b^n\mathbf{f}^b \times \delta\boldsymbol{\theta} + \delta\mathbf{g}^n + \mathbf{C}_b^n\delta\mathbf{f}^b \\ \delta\dot{\boldsymbol{\theta}} = -(\boldsymbol{\omega}_{en}^n + \boldsymbol{\omega}_{ie}^n) \times \delta\boldsymbol{\theta} - \mathbf{C}_b^n\delta\boldsymbol{\omega}_{ib}^b \end{cases} \tag{28}$$

where $\delta\dot{\mathbf{p}}$, $\delta\dot{\mathbf{v}}$, and $\delta\dot{\boldsymbol{\theta}}$ are the derivative of position, velocity, and euler angles vectors, respectively; $\boldsymbol{\omega}_{en}^n$ is the rotation angular rate of n-frame with respect to e-frame projected in n-frame; $\boldsymbol{\omega}_{ie}^n$ is the rotation angular rate of e-frame with respect to inertial i-frame projected in n-frame; $\delta\mathbf{g}^n$ represents the gravity corrections; $\mathbf{f}^b$ and $\boldsymbol{\omega}_{ib}^b$ are the specific force and angular rate from accelerometers and gyroscopes in the b-frame; $\mathbf{C}_b^n$ represents the attitude direction cosine matrix for transforming from b-frame to n-frame; $\delta\mathbf{f}^b$ and $\delta\boldsymbol{\omega}_{ib}^b$ are systematic errors of the accelerometer and gyroscope in b-frame,respectively.

3) Correction step: A GNSS OMC vector in a multi-antenna platform at time k is constructed as

$$\mathbf{y}_k = \mathbf{H}_k\mathbf{x}_{k|k-1} + \mathbf{W}_k \tag{29}$$

in which $\mathbf{x}_{k|k-1}$ is the predicted state vector by IMU. $\mathbf{W}_k$ is the observation noise and assumed to be zero mean Gaussian white noise with covariance $\mathbf{R}_k$, which is constructed based on the observation noise ϵ in (5) and the cross-correlation between the main and secondary antennas has been considered [65]. The OMC vector $\mathbf{y}_k$ and design matrix $\mathbf{H}_k$ can be constructed based on (21) as

$$\begin{cases} \mathbf{y}_k = [\mathbf{y}_m^\top \ \mathbf{y}_{1m}^\top \ \cdots \ \mathbf{y}_{sm}^\top]^\top \\ \mathbf{H}_k = [\mathbf{H}_{\text{kin}} \ \mathbf{H}_{\text{IMU}} \ \mathbf{H}_{\text{GNSS}} \ \mathbf{H}_{\text{a}}] \end{cases}, \tag{30}$$

where

$$\mathbf{H}_{\text{kin}} = \begin{bmatrix} \mathbf{H}_m^{\delta\mathbf{p}} & \mathbf{0} & \mathbf{0} \\ \mathbf{0} & \mathbf{0} & \mathbf{H}_{1m}^{\delta\boldsymbol{\theta}} \\ \vdots & \vdots & \vdots \\ \mathbf{0} & \mathbf{0} & \mathbf{H}_{Nm}^{\delta\boldsymbol{\theta}} \end{bmatrix}, \ \mathbf{H}_{\text{IMU}} = \begin{bmatrix} \mathbf{0} & \mathbf{0} \\ \mathbf{0} & \mathbf{0} \\ \vdots & \vdots \\ \mathbf{0} & \mathbf{0} \end{bmatrix} \tag{31}$$

and

$$\mathbf{H}_{\text{GNSS}} = \begin{bmatrix} \mathbf{H}_m^{\mathbf{o}} \\ \mathbf{0} \\ \vdots \\ \mathbf{0} \end{bmatrix}, \mathbf{H}_{\text{GNSS}} = \begin{bmatrix} \mathbf{H}_m^{\mathbf{a}} & \mathbf{0} & \mathbf{0} & \mathbf{0} \\ \mathbf{0} & \mathbf{H}_{1m}^{\mathbf{a}} & \mathbf{0} & \mathbf{0} \\ \mathbf{0} & \mathbf{0} & \ddots & \mathbf{0} \\ \mathbf{0} & \mathbf{0} & \mathbf{0} & \mathbf{H}_{Nm}^{\mathbf{a}} \end{bmatrix}. \tag{32}$$

The meanings of symbols in (30), (31) and (32) refer to (21). It should be noted that in the GNSS correction step the coefficients corresponding to velocity (the second column of $\mathbf{H}_{\text{kin}}$) and IMU biases ($\mathbf{H}_{\text{IMU}}$) are zeros. In addition, the IMU is directly mounted under the main antenna, thus the level-arm between the IMU and main antennas has been ignored.

The correction step is actually using GNSS measurements to calibrate the state predicted by IMU, the adjustment of state vector and its variance-covariance matrix are obtained by

$$\begin{cases} \hat{\mathbf{x}}_{k|k} = \mathbf{K}_k(\mathbf{y}_k - \mathbf{H}_k\mathbf{x}_{k|k-1}) \\ \mathbf{P}_{k|k} = (\mathbf{I} - \mathbf{K}_k\mathbf{H}_k)\mathbf{P}_{k|k-1} \end{cases}, \tag{33}$$

in which the $\mathbf{K}_k$ is the Kalman gain matrix [66]. The updated state is calculated as

$$\mathbf{x}_{k|k} = \mathbf{x}_{k|k-1} \oplus \hat{\mathbf{x}}_{k|k}, \tag{34}$$

where the symbol $\oplus$ is a generic composition defined in (4).

D. Ambiguity Resolution

After the correction step, we get the solutions without ambiguity resolution named as float solutions:

$$\mathbf{x}_{k|k} = [\mathbf{x}_{\text{kin}}^\top \ \mathbf{x}_{\text{IMU}}^\top \ \mathbf{x}_{\text{GNSS}}^\top \ \mathbf{x}_{\text{a}}^\top]_{k|k}^\top. \tag{35}$$

If we take a close look at (21) and (27), we can see the symbol $\widetilde{\mathbf{a}}_m$ denoting undifferenced ambiguities for main antenna has a tilde, while the double-differenced ambiguities $\mathbf{a}_{1m}$ and $\mathbf{a}_{sm}$ don't. This is because although satellite phase biases have been corrected by SSR products, the undifferenced ambiguities $\widetilde{\mathbf{a}}_m$ still contain the receiver phase biases which have been

mitigated in the double-differenced ambiguities. Therefore, before the ambiguity resolution, we need to transform the undifferenced ambiguities to single-differenced ambiguities between two satellites, so as to eliminate receiver phase biases and recover integer features of the ambiguities for the main antenna. This transformation can be achieved by

$$\hat{\mathbf{x}}_{\bar{\mathrm{a}}} = \mathbf{T}\hat{\mathbf{x}}_{\mathrm{a}} = \begin{bmatrix} \mathbf{U} & \mathbf{0} & \mathbf{0} & \mathbf{0} \\ \mathbf{0} & \mathbf{I} & \mathbf{0} & \mathbf{0} \\ & & \ddots & \\ \mathbf{0} & \mathbf{0} & & \mathbf{0} \\ \mathbf{0} & \mathbf{0} & \mathbf{0} & \mathbf{I} \end{bmatrix} \begin{bmatrix} \widetilde{\mathbf{a}}_m \\ \mathbf{a}_{1m} \\ \vdots \\ \mathbf{a}_{Nm} \end{bmatrix}_{k|k}, \tag{36}$$

where $\mathbf{U}$, constructed according to [27], is an matrix to transform the undifferenced ambiguities $\widetilde{\mathbf{a}}_m$ to single-differenced ambiguities $\overline{\mathbf{a}}_m$. Let $\overline{\mathbf{a}} = [\overline{\mathbf{a}}_m^\top \ \mathbf{a}_{1m}^\top \ \dots \ \mathbf{a}_{Nm}^\top]^\top$ and the corresponding variance-covariance matrix is transformed to

$$\begin{bmatrix} \mathbf{P}_{\text{kin, kin}} & \mathbf{P}_{\text{kin, IMU}} & \mathbf{P}_{\text{kin, GNSS}} & \mathbf{P}_{\text{kin, }\overline{a}} \\ \mathbf{P}_{\text{IMU, kin}} & \mathbf{P}_{\text{IMU, IMU}} & \mathbf{P}_{\text{IMU, GNSS}} & \mathbf{P}_{\text{IMU, }\overline{a}} \\ \mathbf{P}_{\text{GNSS, kin}} & \mathbf{P}_{\text{GNSS, IMU}} & \mathbf{P}_{\text{GNSS, GNSS}} & \mathbf{P}_{\text{GNSS, }\overline{a}} \\ \mathbf{P}_{\overline{a}\text{, kin}} & \mathbf{P}_{\overline{a}\text{, IMU}} & \mathbf{P}_{\overline{a}\text{, GNSS}} & \mathbf{P}_{\overline{a}\text{, }\overline{a}} \end{bmatrix} = \begin{bmatrix} \mathbf{I} & \mathbf{0} & \mathbf{0} & \mathbf{0} \\ \mathbf{0} & \mathbf{I} & \mathbf{0} & \mathbf{0} \\ \mathbf{0} & \mathbf{0} & \mathbf{I} & \mathbf{0} \\ \mathbf{0} & \mathbf{0} & \mathbf{0} & \mathbf{T} \end{bmatrix} \mathbf{P}_{k|k} \begin{bmatrix} \mathbf{I} & \mathbf{0} & \mathbf{0} & \mathbf{0} \\ \mathbf{0} & \mathbf{I} & \mathbf{0} & \mathbf{0} \\ \mathbf{0} & \mathbf{0} & \mathbf{I} & \mathbf{0} \\ \mathbf{0} & \mathbf{0} & \mathbf{0} & \mathbf{T} \end{bmatrix}^\top. \tag{37}$$

Then, the ambiguity vector $\mathbf{x}_{\overline{a}}$ and its covariance $\mathbf{P}_{\overline{a},\overline{a}}$ are used for ambiguity resolution.

The C-LAMBDA, MC-LAMBDA, and AC-LAMBDA methods mentioned in Section II mainly focus on ambiguity solution in unaided, single frequency, single epoch cases, and the difficulty of computing and estimating the integer ambiguities depends very much on the strength of the underlying model. In the unaided, single frequency, single epoch case, the mathematical models lack the necessary strength. Therefore, additional prior information, such as baseline length and orthonormality of the rotation matrix, is often used in case of attitude determination to strengthen the ambiguity resolution. However, we focus on IMU-aided, double-frequency, multi-epoch GPS+Galileo ambiguity resolution. Clearly, the strength of the GNSS mathematical model is improved when aided by IMU, when the number of tracked satellites gets larger, when the number of measurement epochs increases, and when used frequencies gets more. In addition, the baseline length constraints have been fulfilled by transforming the coordinate difference to quaternion in the observational models, and the quadratic constraints has been removed in the linearization of the quaternion. In such cases the models have sufficient strength, the standard LAMBDA methods can be used directly for ambiguity resolution [42]. This has been proven that the differences in success rate between classical LAMBDA and MC-LAMBDA become less pronounced when the strength of the underlying GNSS model increases. For instance, with 8 satellites and a phase and code precision of 3 mm and 5 cm, respectively, a close to 100% success rate is already achieved with the standard LAMBDA method [43]. Therefore, we finally choose the standard LAMBDA method to avoid the computational complexity of MC-LAMBDA while also achieving a comparable success rate of ambiguity resolution with a strengthened mathematical model.

Once the ambiguity is successfully resolved to an integer vector $\mathbf{x}_a$, the position, velocity, and attitude solutions with ambiguity resolution, named as fixed solutions, can be derived as

$$\mathbf{x}_{\text{kin}} = \mathbf{x}_{\text{kin}} \oplus \mathbf{P}_{a,\text{kin}}\mathbf{P}_{a,a}^{-1}(\mathbf{x}_a - \hat{\mathbf{x}}_a), \tag{38}$$

where the meaning of the operator $\oplus$ can be found in (4).

V. Experimental Setup and Data Collection

A. Setup of Platform

We installed the multi-sensor platform on our research boat *Aurora*. Aurora carries one tactical grade IMU and three geodetic antennas as shown in Fig. 4. The three antennas are connected to three JAVAD GNSS receivers. The main antenna is mounted at the bow of the boat with the IMU directly below it. Two secondary antennas are mounted at the left and right edges of Aurora's roof. The definition of the whole body frame (b-frame) is illustrated in Fig. 4: the origin point of b-frame is the main antenna and the positions of the two secondary antennas in b-frame are determined based on the geometric information. From Fig. 4, we know the $(Front, Right, Down)$ coordinates in b-frame for the left and right secondary antennas are $(-1.682, -0.687, -0.194)$ and $(-1.682, 0.540, -0.194)$.

B. Measurement Campaign

We conducted a measurement campaign on the urban waterways of Berlin on November 8, 2022. Between 2:30 pm and 4:30 pm, the boat moved around the small island *Seestraßeninsel*. In total, it passed seven times around the island and 18 times under bridges. Fig. 4 illustrates the trajectory. During this measurement campaign, we were receiving SSR corrections of satellite orbit, clock, and signal biases as well as tropospheric and ionospheric delays from SAPOS. The SSR products were generated based on 11 reference stations located near Berlin, as shown by the black circles in Fig. 5. Close to the location of the measurement campaign, we also chose an RTK base station, indicated as red diamond in Fig. 5. This base station serves for computing RTK solutions as references. With these references, section VI evaluates the positioning performance of the Array PPP-RTK method.

C. Data Processing Strategies

Table I shows the processing strategies. The GNSS receivers have the capability to track and receive GPS, Galileo and GLONASS satellites and signals, but only GPS and Galileo are implemented for Array PPP-RTK because the decode of SSR corrections for GLONASS is under development. We are using a tactical grade IMU (Sensonor STIM300). Based on the specifications of IMU sensor, its configurations have been modified.

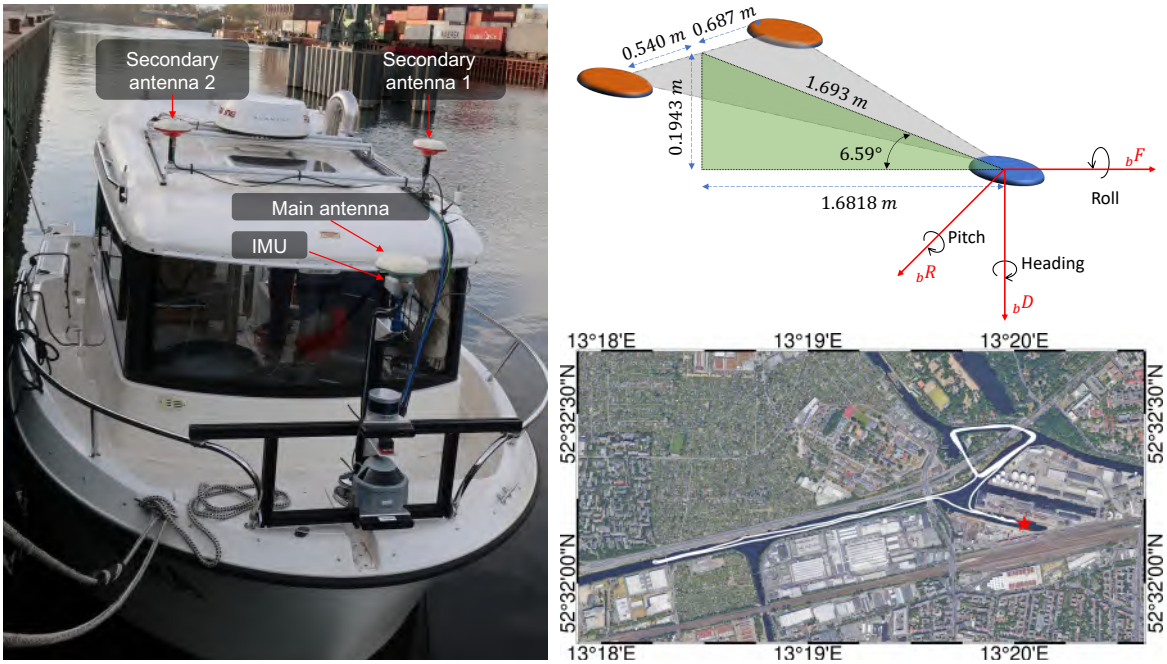

Fig. 4. On the left, the research vessel Aurora and its multi-antenna and multi-sensor platform. On the top right, side view of the geometric structure and the inter-antenna baselines in the body frame. On the bottom right, the trajectory of the measurement campaign, the red star marks the start and stop point.

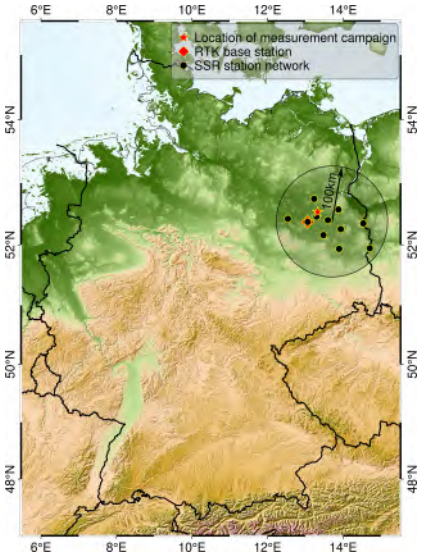

Fig. 5. Reference stations used by SAPOS to generate SSR corrections

TABLE I
DATA PROCESSING AND CONFIGURATION FOR ARRAY PPP-RTK.

GNSS items	Processing strategies
GNSS signals	GPS (L1, L2) Galileo (E1, E5a)
Observation noise	Elevation dependent: $(\frac{\sigma}{sin(Elev)})^2$, where σ for code measurement is 0.6 m and for phase measurement is 0.01 cycle
Sampling rate	2 Hz
Elevation mask	15°
Ambiguities	Resolved by Partial-LAMBDA and minimum success rate is set as 99.5%
Satellite orbit, clock, and signal biases	Corrected by SSR products from SAPOS
Atmospheric delays	Mitigated in the double-differencing operation for secondary antennas. Estimate residual iono-spheric and tropospheric delays with respect to SSR atmospheric products for main antenna

VI. RESULTS ANALYSIS

As explained in the introduction, position and attitude are two key aspects of precise navigation. Thus, the first part focuses on the performance of the positioning results, especially the precision and convergence time, whereas the second part presents the performance of the attitude estimation in terms of accuracy and rapid initialization.

A. Positioning Performances

As mentioned in Section V-B, an RTK reference trajectory is obtained by using RTKLib [67] with an RTK base station visible in Fig. 5. The configuration parameters of the RTKLib processor are described in Table II. It is worth noting that GLONASS were also used in addition to GPS and Galileo to generate the reference trajectory. This was fundamental to increase the availability of satellites during passing through bridges, increasing the reliability of RTK solutions. Moreover, RTK solutions are computed based on final orbit and clock products from Center for Orbit Determination in Europe (CODE), which are generated based on a global station network. The SSR orbit and clocks applied by PPP-RTK are determined based on a regional station network. As a result, there exists positioning offset between PPP-RTK and RTK solutions. This positioning offset is calculated by averaging the

TABLE II
DATA PROCESSING STRATEGIES OF RTK SOLUTIONS

Items	Processing strategies
GNSS signals	GPS(L1, L2), GLONASS(G1, G2), Galileo(E1, E5a)
Observation noise	Elevation dependent: $a^2 + (b/sin(Elev))^2$ where $a = 0.002$ m and $b = 0.002$ m, the noise ratio between code and phase measurements is 100
Sampling rate	2 Hz
Elevation mask	15°
Ambiguities	Resolve GPS and Galileo ambiguities by LAMBDA, ratio test threshold is set as 2; Keep GLONASS ambiguities as float values
Satellite orbit, clock, and signal biases	Apply precise satellite orbit and clock from CODE, and signal biases are mitigated in the double-differenced observations
Atmospheric delays	Reduced in the double-differenced observations and ignored

positioning differences between PPP-RTK and RTK solutions, and removed in the evaluation analysis [27].

To highlight the performance improvement of the Array PPP-RTK algorithm with the fusion of multi-antenna and IMU, two additional solutions have been computed: (a) a PPP-RTK solution with the main antenna only; (b) a tightly coupled PPP-RTK and IMU solution based on single main antenna. The solution (c) presents the tightly coupled Array PPP-RTK and IMU solutions. A comparison between them is analyzed in the following.

1) Positioning precision: The trajectory comparison for different types of solutions is presented in Fig. 6. Based on the SSR products, the PPP-RTK solutions (a) always realized rapid ambiguity resolution within seconds even after passing through the bridges. For this reason, the convergence time of the positioning solution is also strongly reduced as it is visible in Fig. 7a, which presents the errors in the East-North coordinate frame. The main disadvantage of PPP-RTK is also obvious and visible in Fig. 6a, i.e. it cannot provide continuous solutions during passing through a bridge. Additionally, in the vicinity of the bridges the error tends to be larger due to multi-path signals and potential cycle slips. This motivates the integration of the IMU sensor which compensates the unavailability of GNSS signals during passing through a bridge. The solutions (b) with tightly coupled PPP-RTK and IMU not only provide continuously positioning results under the bridges, but also improve the fixing rate of ambiguity resolution. The fixing rate here defined as the ratio between the fixed epochs and the total epochs. The total epochs here also include the epochs when there is not available GNSS satellites at all and only IMU works, e.g., when the boat is under a bridge. The fixing rate increased from 98.6% in solution (a) to 99.4% in solution (b). Although the increase is small, the improvement mainly occurs during crossing bridges, which can be observed through the comparison of red dots in Fig. 7b and Fig. 7a especially at time 16:20. This is important to enhance the reliability of the positioning and reduce the initialization time. Therefore, the IMU integration reduces the time to obtain fixed solutions lowering down the positioning errors. From solution (b) to solution (c), two secondary antennas are added. The cross correlation between the three antennas is considered and the fixing rate increased to 99.5%. Even though the contribution to positioning precision is minor, the main benefit is visible on the attitude estimation which will be discussed in Section VI-B.

TABLE III
STANDARD DEVIATIONS OF ERRORS FOR DIFFERENT SOLUTIONS IN THE EAST AND NORTH COMPONENTS

Solution type	RMS	
	East	North
Solution (a)	0.132 m	0.084 m
Solution (b)	0.090 m	0.073 m
Solution (c)	0.055 m	0.058 m

The horizontal positioning errors compared with the reference RTK solutions in the east and north components are presented in Fig. 7. For all the three types of solutions, the positioning errors are lower than 0.1 m in open-sky areas. In total, the boat passed through bridges 18 times, and most of the large position errors are observed shortly after the bridge crossings. To quantify the error, the standard deviations of errors in the east and north directions are used to evaluate the precision, as listed in Table III . For the solution (a), the standard deviations of errors in the east and north components are 0.132 m and 0.084 m, respectively. With the integration of IMU (solution (b)), the standard deviations decreased to 0.090 m and 0.073 m. Additionally, the visible large errors in solution (a) after crossing bridges are considerably reduced in solution (b). The Solution (c) introduces multi-antenna system, which helps to calibrate the attitude determination of IMU. The accurate attitude information in turn improves the IMU-derived positioning results. Thus, the standard deviations of solution (c) are further improved to 0.055 m and 0.058 m in east and north components. As it is visible in Fig. 6 and 7, and by considering standard deviations of errors in the east and north components, it appears clear that the Array PPP-RTK with multi-antenna and IMU integration considerably improves the positioning precision, especially in GNSS-denied environments. The achieved precision in the positioning domain largely satisfies the positioning requirements of many intelligent transportation applications.

2) Convergence time: Many applications require fast convergence time within a few seconds. Thus, in addition to positioning precision, the convergence time is considered as another performance indicator and evaluated for the three types of solutions. In this manuscript, the convergence time is defined as the time the horizontal positioning errors starts to be better than 0.1 m and stays within 0.1 m for the next 10 epochs [27]. The boat passed bridges 18 times, and we evaluated the convergence time over these times. The results are listed in Table IV, where the convergence time t is grouped in 4 different time-bins in seconds: $t \in [0, 5]$, $t \in (5, 10]$, $t \in (10, 15]$, and $t > 15$. In solution (a), 10 of 18 samples

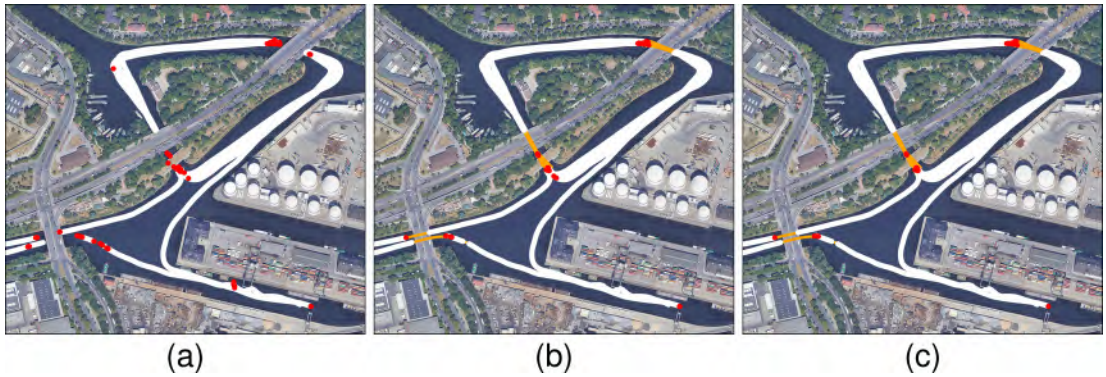

Fig. 6. Trajectory comparison for different types of solutions: (a) PPP-RTK using the main antenna only; (b) Tightly coupled PPP-RTK and IMU solutions based on single main antenna; (c) Tightly coupled Array PPP-RTK and IMU solutions based on three antennas. The white and red colors mean fixed and float solutions, respectively. The orange colors in (b) and (c) means IMU derived positions where GNSS is unavailable.

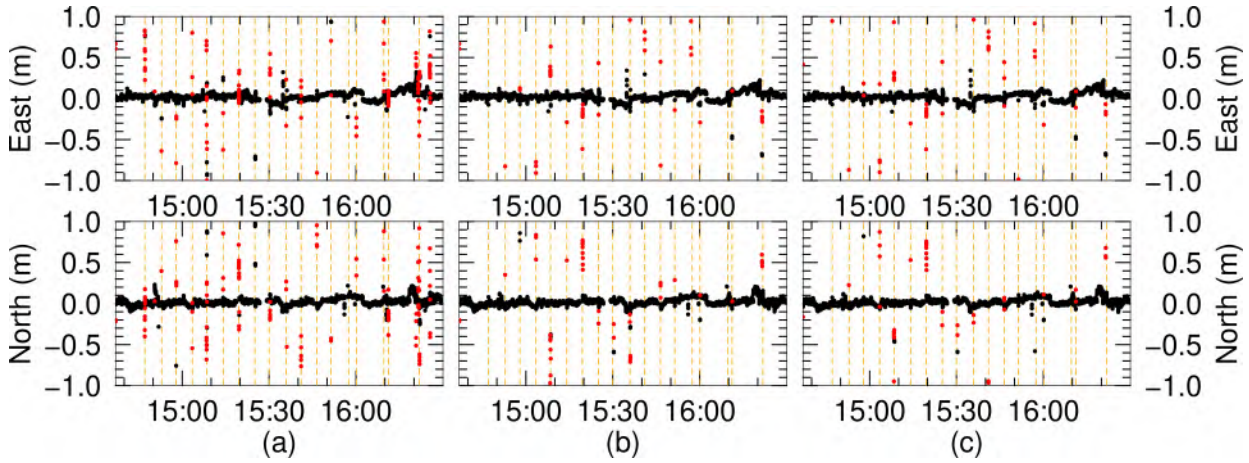

Fig. 7. Horizontal positioning errors of three types of solutions compared with RTK solutions: (a) PPP-RTK using the main antenna only; (b) Tightly coupled PPP-RTK and IMU solutions based on the single main antenna; (c) Tightly coupled Array PPP-RTK and IMU solutions based on the three antennas. The red and black colors denote the float and fixed solutions, respectively. The orange dashed vertical lines mark the time of passing through bridges.

achieved rapid convergence with an average time of 3 s for the time-bin $t \in [0, 5]$; As for $t \in (5, 10]$, there were 5 samples with an average time of 8.2 s, and 2 samples took more than 15 s to converge. From solution (a) to solution (b), the samples with $t \in [0, 5]$ was increased by 1, meanwhile the average convergence time of this time-bin was reduced from 3 s to 2 s. Moreover, 5 samples had an average convergence time of 8.1 s for $t \in (10, 15]$ and the longest convergence time was 18 s. With regards to solution (c), the samples with $t \in [0, 5]$ was increased to 12 with an average of 1.5 s. For $t \in (5, 10]$, the average time of 5 samples was 7.9 s and only one sample had a convergence time of 18 s. In summary, PPP-RTK is characterized by a rapid convergence time. For the solution (a), 15 of the 18 samples converged within 10 seconds, whereas when an IMU was integrated 16 over the 18 samples converged within 10 s. Last but not least, when multiple GNSS antennas were used in combination with the IMU, 17 of the 18 samples converged rapidly within 10 s showing the benefits of the proposed approach.

TABLE IV
CONVERGENCE TIME FOR DIFFERENT TYPES OF SOLUTIONS.

Convergence time (s)	Number of samples (Average time)			
	$0 < t \leq 5$	$5 < t \leq 10$	$10 < t \leq 15$	$t > 15$
Solution (a)	10 (3.0 s)	5 (8.2 s)	1 (15.0 s)	2 (19.0 s)
Solution (b)	11 (2.0 s)	5 (8.1 s)	1 (14.0 s)	1 (18.0 s)
Solution (c)	12 (1.5 s)	5 (7.9 s)	0 (-)	1 (18.0 s)

B. Performances of Attitude Determination

The attitude solution estimated by Array PPP-RTK method in the multi-antenna, multi-sensor platform is illustrated in Fig. 8. The roll and pitch varied around zero, and heading ranges from -180° to 180°. The boat turned around within seconds at 16:10, thus there was a 180° change of heading at that time. What we should note is that benefiting from IMU integration the Array PPP-RTK method can continuously provide attitude solutions even during passing through the bridges. In other words, it improves the solution continuity and availability in a harsh environment.

To evaluate the attitude estimation process, an accurate reference is needed. The optimal way to obtain a reference attitude information is using a navigation grade IMU with a precise attitude initialization. However, the navigation grade

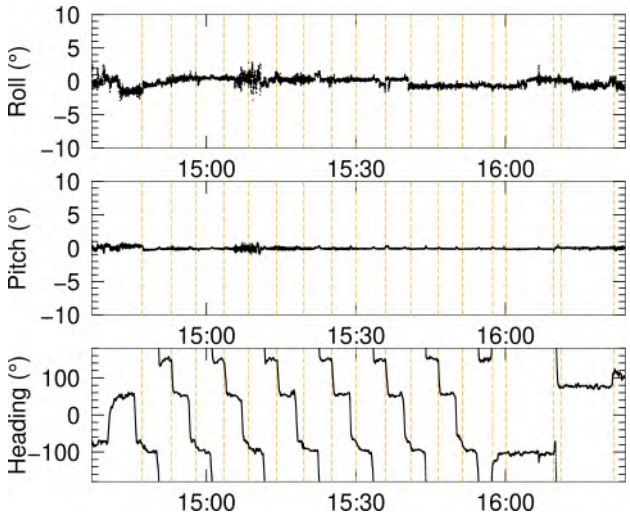

Fig. 8. Attitude solution estimated by Array PPP-RTK method in the multi-antenna, multi-sensor system. The orange dashed vertical lines indicate the time of crossing bridges.

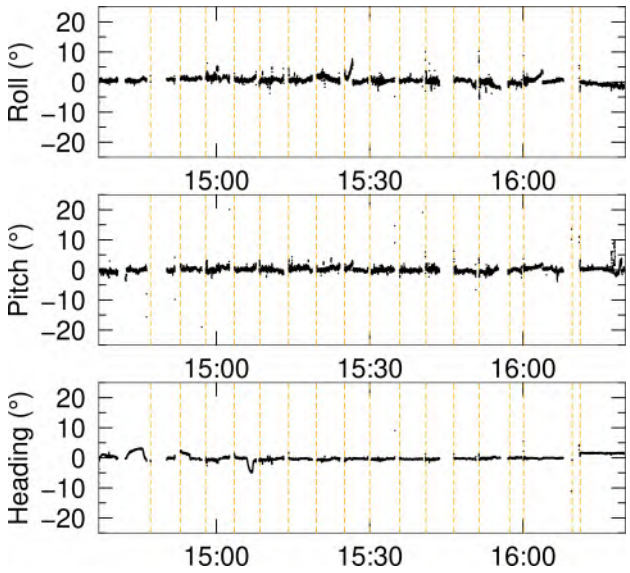

Fig. 9. Attitude difference between Array PPP-RTK and RTK methods. The orange dashed vertical lines indicate the time of crossing bridges.

IMU was not available in this measurement campaign. As an alternative approach, the moving-baseline solution provided by RTKLib was used to estimate attitude information. The attitude accuracy derived by this RTK method not only depends on the RTK accuracy but also the baseline length. Given a baseline length of 1.7 m and assuming the horizontal and vertical accuracy of RTK solution is 0.02 m and 0.05 m, the expected attitude accuracies are $0.02/1.7\times180^\circ/\pi = 0.67^\circ$ for heading and $0.05/1.7 \times 180^\circ/\pi = 1.69^\circ$ for pitch and roll. Fig. 9 presents the differences of the roll, pitch and heading angles between the Array PPP-RTK and RTK methods. As it is visible, some data gaps are present in the results due to the fact that the RTK method cannot continuously generate attitude information when GNSS signals are obstructed by the bridges. Some large attitude discrepancies are observed just before and after the bridge crossing. The standard deviations of the attitude differences are 1.56°, 2.03° and 0.86° in roll, pitch and heading. As expected, the standard deviations of roll and pitch is larger than that of heading, because their computation depends on the vertical component, while heading is based on horizontal components. As is known, RTK solutions have a rapid convergence of several seconds. Benefiting from the multi-antenna system, the Array PPP-RTK method provided continuous attitude solutions under bridges and also achieved rapid convergence, which can be seen from the initialization at the beginning and re-initialization after passing the bridges.

PPP-RTK and IMU integrated on one antenna (solution (b) in Section VI-A) can also generate attitude information. However, in this case the initialization of the attitude plays a crucial role to obtain fast reliable solution. If no prior attitude information is available, the expected convergence time is quite long. With this regard, the usage of the multi-antenna system provides an initial accurate attitude estimation by drastically reducing the convergence time of the estimation process. To highlight the contribution of multi-antenna system to the attitude determination, we compared the PPP-RTK and IMU attitude determination in single-antenna and multi-antenna system, as presented in Fig. 10. It can be seen that the heading estimation with a single antenna required approximately 40 minutes to converge to a stable solution due to the large error (approximately 100 degrees) in the initialization process. If the initial attitude information is not known in advance, the error on the heading may range from -180 to 180 degrees. On the other hand, if the initial attitude error is small, the convergence time is dramatically reduced, and a stable and accurate information can be retrieved. For instance, this can be observed for the pitch and roll estimation presented in Fig. 10. The actual pitch and roll for the boat are clearly close to zero, thus by initializing the filter with zero pitch and roll angles provided a good initial estimates with small errors and lowered down the convergence time. For such a reason, the usage of the multi-antenna system provides a good initial attitude estimation which significantly reduces the convergence time of the provided solution.

VII. Conclusions and Outlooks

We derived a quaternion-based unified mathematical model for Array PPP-RTK with tight integration of IMU in a multi-antenna system, achieving continuous and precise joint positioning and attitude determination. The corresponding performances have been evaluated with a real data set collected from a measurement campaign. The results demonstrate that the fixing rate of the ambiguities achieved 99.5%, the precision of positioning errors are 0.055 m and 0.058 m in the east and north components. The boat crossed bridges 18 times and in 17 of the 18 cases the horizontal positioning errors converged to 10 cm within 10 seconds. In terms of attitude, the multiple antennas facilitate the initial alignment of IMU and the convergence time of heading is significantly reduced from 40 minutes with a single antenna to a few seconds with a multi-antenna system. Thus, the Array PPP-RTK method based on a multi-antenna, multi-sensor platform is capable

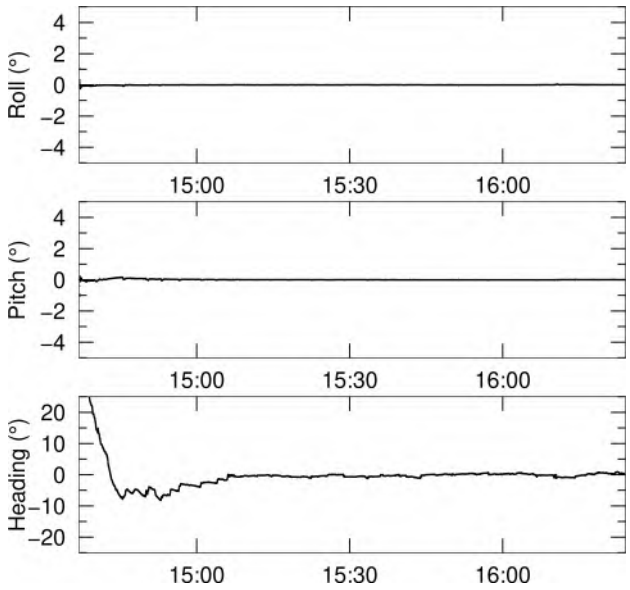

Fig. 10. PPP-RTK and IMU attitude determination on a single antenna compared with that in a multi-antenna system.

of providing continuous and precise positioning and attitude information for intelligent vehicles.

Considering the complexities of automated navigation especially in a harsh environment, the Array PPP-RTK method could be improved and optimized in the following aspects:

- Compute a more accurate attitude as reference for evaluation and validation. Install a navigation grade IMU within this platform and assign accurate initial attitude, so that to get accurate attitude information to assess the results.
- Tune between GNSS and IMU. The Array PPP-RTK method is based on a multi-sensor platform, the contribution of different sensors to Array PPP-RTK should be tuned and optimized according to the specifications of the sensor, especially for IMU.
- Tune between different parameters. The process noise of different parameters should also be optimized according to the dynamic characteristics of the parameters and target applications. For example, the process noise of roll and pitch should be smaller than the heading, because the roll and pitch angles usually fluctuate around zero and vary a little for the land vehicle application.
- Mitigate the effects of Non Line-Of-Sight (NLOS) signals aided by LiDAR and Camera. As you may have noticed in Fig. 4, the research boat is a multi-sensor platform including also LiDAR and Camera sensors. For transportation applications, the vehicle usually drives in an urban area where exists a lot NLOS signals. The NLOS signals is an error source for GNSS data processing in harsh environments. With the perception information collected by LiDar and Camera, we can detect and exclude GNSS NLOS signals.

ACKNOWLEDGMENTS

We thank SAPOS and GEO++ for the provision of SSR correction data. We also acknowledge Center of Orbit Determination in Europe (CODE) for offering the precise satellite orbit and clock products. Last but not the least, we acknowledge anonymous reviewers for their valuable, constructive, and prompt comments.

REFERENCES

[1] D. Medina, "Robust GNSS Carrier Phase-based Position and Attitude Estimation," Ph.D. dissertation, Universidad Carlos III de Madrid, 2022.

[2] H. Caesar, V. Bankiti, A. H. Lang, S. Vora, V. E. Liong, Q. Xu, A. Krishnan, Y. Pan, G. Baldan, and O. Beijbom, "nuScenes: A Multimodal Dataset for Autonomous Driving," in *Proceedings of the IEEE/CVF conference on computer vision and pattern recognition*, 2020, pp. 11 621–11 631.

[3] W. Wen, Y. Zhou, G. Zhang, S. Fahandezh-Saadi, X. Bai, W. Zhan, M. Tomizuka, and L.-T. Hsu, "UrbanLoco: A full sensor suite dataset for mapping and localization in urban scenes," in *2020 IEEE international conference on robotics and automation (ICRA)*. IEEE, 2020, pp. 2310–2316.

[4] W. Maddern, G. Pascoe, C. Linegar, and P. Newman, "1 year, 1000 km: The Oxford RobotCar Dataset," *The International Journal of Robotics Research*, vol. 36, no. 1, pp. 3–15, 2017.

[5] Y. Choi, N. Kim, S. Hwang, K. Park, J. S. Yoon, K. An, and I. S. Kweon, "KAIST multi-spectral day/night data set for autonomous and assisted driving," *IEEE Transactions on Intelligent Transportation Systems*, vol. 19, no. 3, pp. 934–948, 2018.

[6] A. Geiger, P. Lenz, and R. Urtasun, "Are we ready for Autonomous Driving? The KITTI Vision Benchmark Suite," in *2012 IEEE conference on computer vision and pattern recognition*. IEEE, 2012, pp. 3354–3361.

[7] G. Wübbena, M. Schmitz, and A. Bagge, "Ppp-rtk: precise point positioning using state-space representation in rtk networks," in *Proceedings of the 18th international technical meeting of the satellite division of the Institute of navigation (ION GNSS 2005)*, 2005, pp. 2584–2594.

[8] J. Geng, F. Teferle, X. Meng, and A. Dodson, "Towards ppp-rtk: Ambiguity resolution in real-time precise point positioning," *Advances in Space Research*, vol. 47, no. 10, pp. 1664–1673, 2011, gNSS Remote Sensing-2. [Online]. Available: https://www.sciencedirect.com/science/article/pii/S0273117710002498

[9] P. J. Teunissen, "A-ppp: Array-aided precise point positioning with global navigation satellite systems," *IEEE Transactions on Signal Processing*, vol. 60, no. 6, pp. 2870–2881, 2012.

[10] P. J. G. Teunissen, "The least-squares ambiguity decorrelation adjustment: a method for fast gps integer ambiguity estimation," *Journal of Geodesy*, vol. 70, no. 1, pp. 65–82, Nov 1995. [Online]. Available: https://doi.org/10.1007/BF00863419

[11] P. Teunissen, "The probability distribution of the GPS baseline for a class of integer ambiguity estimators," *Journal of Geodesy*, vol. 73, pp. 275–284, 1999.

[12] D. Medina, J. Vilà-Valls, E. Chaumette, F. Vincent, and P. Closas, "Cramér-Rao bound for a mixture of real-and integer-valued parameter vectors and its application to the linear regression model," *Signal Processing*, vol. 179, p. 107792, 2021.

[13] H. Wymeersch, R. Amiri, and G. Seco-Granados, "Fundamental Performance Bounds for Carrier Phase Positioning in Cellular Networks," *arXiv preprint arXiv:2306.12133*, 2023.

[14] S. Yan and Y.-B. Li, "High-precision satellite positioning device on the basis of triangle receiver array and positioning method," Oct. 2017, cN Patent 105 549 048.

[15] J. Ji, W. Chen, J.-T. Zhang, Y. Shen, Y.-B. Li, and L.-Y. Du, "Comparsion of vehicle positioning performance based on rac technology," in *2019 5th International Conference on Transportation Information and Safety (ICTIS)*, 2019, pp. 805–809.

[16] J. Ji, J. Zhang, H. Lu, Y. Liu, D. Wu, and W. Chen, "A single-frequency real-time lane-level positioning method for vehicle safety," *IEEE Access*, vol. 8, pp. 185 651–185 664, 2020.

[17] EUSPA, "Report on road user needs and requirements: Outcome of the euspa user consultation platform," EUSPA, Tech. Rep., Sep 2021. [Online]. Available: https://www.gsc-europa.eu/sites/default/files/sites/all/files/Report_on_User_Needs_and_Requirements_Road.pdf

[18] S. Malys and P. A. Jensen, "Geodetic point positioning with gps carrier beat phase data from the casa uno experiment," *Geophysical Research Letters*, vol. 17, no. 5, pp. 651–654, 1990. [Online]. Available: https://agupubs.onlinelibrary.wiley.com/doi/abs/10.1029/GL017i005p00651

[19] J. F. Zumberge, M. B. Heflin, D. C. Jefferson, M. M. Watkins, and F. H. Webb, "Precise point positioning for the efficient and robust analysis of gps data from large networks," *Journal of Geophysical Research: Solid Earth*, vol. 102, no. B3, pp. 5005–5017, 1997. [Online]. Available: https://agupubs.onlinelibrary.wiley.com/doi/abs/10.1029/96JB03860

[20] V. Janssen, "A comparison of the vrs and mac principles for network rtk. international global navigation satellite systems society," in *IGNSS Symposium 2009*, 2009.

[21] P. J. G. Teunissen, R. Odolinski, and D. Odijk, "Instantaneous beidou+gps rtk positioning with high cut-off elevation angles," *Journal of Geodesy*, vol. 88, no. 4, pp. 335–350, Apr 2014. [Online]. Available: https://doi.org/10.1007/s00190-013-0686-4

[22] P. J. Teunissen, *GNSS Precise Point Positioning*. John Wiley & Sons, Ltd, 2020, ch. 20, pp. 503–528. [Online]. Available: https://onlinelibrary.wiley.com/doi/abs/10.1002/9781119458449.ch20

[23] J. Aggrey and S. Bisnath, "Improving gnss ppp convergence: The case of atmospheric-constrained, multi-gnss ppp-ar," *Sensors*, vol. 19, no. 3, 2019. [Online]. Available: https://www.mdpi.com/1424-8220/19/3/587

[24] C. Cai, Y. Gong, Y. Gao, and C. Kuang, "An approach to speed up single-frequency ppp convergence with quad-constellation gnss and gim," *Sensors*, vol. 17, no. 6, 2017. [Online]. Available: https://www.mdpi.com/1424-8220/17/6/1302

[25] H. Zhang, Z. Gao, M. Ge, X. Niu, L. Huang, R. Tu, and X. Li, "On the convergence of ionospheric constrained precise point positioning (ic-ppp) based on undifferential uncombined raw gnss observations," *Sensors*, vol. 13, no. 11, pp. 15 708–15 725, 2013. [Online]. Available: https://www.mdpi.com/1424-8220/13/11/15708

[26] P. J. G. Teunissen and A. Khodabandeh, "Review and principles of ppp-rtk methods," *Journal of Geodesy*, vol. 89, no. 3, pp. 217–240, Mar 2015. [Online]. Available: https://doi.org/10.1007/s00190-014-0771-3

[27] X. An, R. Ziebold, and C. Lass, "From rtk to ppp-rtk: towards real-time kinematic precise point positioning to support autonomous driving of inland waterway vessels," *GPS Solutions*, vol. 27, no. 2, p. 86, Mar 2023. [Online]. Available: https://doi.org/10.1007/s10291-023-01428-2

[28] O. J. Woodman, "An introduction to inertial navigation," University of Cambridge, Computer Laboratory, Tech. Rep. UCAM-CL-TR-696, Aug. 2007. [Online]. Available: https://www.cl.cam.ac.uk/techreports/UCAM-CL-TR-696.pdf

[29] X. Li, X. Li, J. Huang, Z. Shen, B. Wang, Y. Yuan, and K. Zhang, "Improving ppp–rtk in urban environment by tightly coupled integration of gnss and ins," *Journal of Geodesy*, vol. 95, no. 12, p. 132, Nov 2021. [Online]. Available: https://doi.org/10.1007/s00190-021-01578-6

[30] X. Li, X. Li, S. Li, Y. Zhou, M. Sun, Q. Xu, and Z. Xu, "Centimeter-accurate vehicle navigation in urban environments with a tightly integrated ppp-rtk/mems/vision system," *GPS Solutions*, vol. 26, no. 4, p. 124, Aug 2022. [Online]. Available: https://doi.org/10.1007/s10291-022-01306-3

[31] D.-H. Hwang, S. H. Oh, S. J. Lee, C. Park, and C. Rizos, "Design of a low-cost attitude determination gps/ins integrated navigation system," *GPS Solutions*, vol. 9, no. 4, pp. 294–311, Nov 2005. [Online]. Available: https://doi.org/10.1007/s10291-005-0135-9

[32] C. Eling, L. Klingbeil, and H. Kuhlmann, "Real-time single-frequency gps/mems-imu attitude determination of lightweight uavs," *Sensors*, vol. 15, no. 10, pp. 26 212–26 235, 2015. [Online]. Available: https://www.mdpi.com/1424-8220/15/10/26212

[33] A. I. Chouaib, B. Mohiedin Wainakh, and C. W. Khalaf, "Robust self-corrective initial alignment algorithm for strap-down ins," in *2015 10th Asian Control Conference (ASCC)*, 2015, pp. 1–6.

[34] C. Tan, X. Zhu, Y. Su, Y. Wang, Z. Wu, and D. Gu, "A new analytic alignment method for a sins," *Sensors*, vol. 15, no. 11, pp. 27 930–27 953, 2015. [Online]. Available: https://www.mdpi.com/1424-8220/15/11/27930

[35] A. Khodabandeh and P. J. G. Teunissen, "Array-based satellite phase bias sensing: theory and gps/beidou/qzss results," *Measurement Science and Technology*, vol. 25, no. 9, p. 095801, jul 2014. [Online]. Available: https://dx.doi.org/10.1088/0957-0233/25/9/095801

[36] ——, "Array-aided multifrequency gnss ionospheric sensing: Estimability and precision analysis," *IEEE Transactions on Geoscience and Remote Sensing*, vol. 54, no. 10, pp. 5895–5913, 2016.

[37] B. Li and P. J. G. Teunissen, "Gnss antenna array-aided cors ambiguity resolution," *Journal of Geodesy*, vol. 88, no. 4, pp. 363–376, Apr 2014. [Online]. Available: https://doi.org/10.1007/s00190-013-0688-2

[38] H.-n. Wang and J.-d. Ying, "LAMBDA method for rigid body attitude determination based on GPS," *Acta Aeronautica et Asronautica Sinica*, vol. 22, no. 1, pp. 61–63, 2001.

[39] A. Hauschild, G. Grillmayer, O. Montenbruck, M. Markgraf, and P. Vörsmann, "Gps based attitude determination for the flying laptop satellite," in *Small satellites for earth observation*. Springer, 2008, pp. 211–220.

[40] L. Vander Kuylen, F. Boon, and A. Simsky, "Attitude determination methods used in the polarx2@ multi-antenna GPS receiver," *Proceedings of ION-GPS 2005*, 2005.

[41] P. Teunissen, "The lambda method for the gnss compass," *Artificial Satellites: journal of planetary geodesy*, vol. 41, no. 3, pp. 89–103, 2006, niet eerder opgevoerd dus alsnog opgeven in 2007.

[42] P. J. G. Teunissen, "Integer least-squares theory for the gnss compass," *Journal of Geodesy*, vol. 84, no. 7, pp. 433–447, Jul 2010. [Online]. Available: https://doi.org/10.1007/s00190-010-0380-8

[43] G. Giorgi, P. Teunissen, and P. Buist, "A search and shrink approach for the baselne constrained lambda method: experimental results," in *International Symposium on GPS/GNSS 2008. Toward a new era of positioning technology*, A. Yasuda, Ed. Tokyo University of marine science and technology, 2008, pp. 797–806, null ; Conference date: 11-11-2008 Through 14-11-2008.

[44] G. Giorgi and P. J. G. Teunissen, "Carrier phase gnss attitude determination with the multivariate constrained lambda method," in *2010 IEEE Aerospace Conference*, 2010, pp. 1–12.

[45] G. Giorgi, P. J. Teunissen, S. Verhagen, and P. J. Buist, "Testing a new multivariate gnss carrier phase attitude determination method for remote sensing platforms," *Advances in Space Research*, vol. 46, no. 2, pp. 118–129, 2010, gNSS Remote Sensing-1. [Online]. Available: https://www.sciencedirect.com/science/article/pii/S0273117710001419

[46] G. Giorgi, P. J. G. Teunissen, S. Verhagen, and P. J. Buist, "Instantaneous ambiguity resolution in global-navigation-satellite-system-based attitude determination applications: A multivariate constrained approach," *Journal of Guidance, Control, and Dynamics*, vol. 35, no. 1, pp. 51–67, 2012. [Online]. Available: https://doi.org/10.2514/1.54069

[47] N. Nadarajah, P. J. G. Teunissen, and N. Raziq, "Instantaneous gps–galileo attitude determination: Single-frequency performance in satellite-deprived environments," *IEEE Transactions on Vehicular Technology*, vol. 62, no. 7, pp. 2963–2976, 2013.

[48] P. J. G. Teunissen, "The affine constrained GNSS attitude model and its multivariateinteger least-squares solution," *Journal of Geodesy*, vol. 86, no. 7, pp. 547–563, Jul. 2012.

[49] G. Giorgi and P. J. G. Teunissen, "Multivariate gnss attitude integrity: The role of affine constraints," in *VIII Hotine-Marussi Symposium on Mathematical Geodesy*, N. Sneeuw, P. Novák, M. Crespi, and F. Sansò, Eds. Cham: Springer International Publishing, 2016, pp. 309–315.

[50] B. Li and P. J. G. Teunissen, "Real-time kinematic positioning using fused data from multiple gnss antennas," in *2012 15th International Conference on Information Fusion*, 2012, pp. 933–938.

[51] W. Li, N. Nadarajah, P. J. G. Teunissen, A. Khodabandeh, and Y. Chai, "Array-aided single-frequency state-space rtk with combined gps, galileo, irnss, and qzss l5/e5a observations," *Journal of Surveying Engineering*, vol. 143, no. 4, p. 04017006, 2017. [Online]. Available: https://ascelibrary.org/doi/abs/10.1061/%28ASCE%29SU.1943-5428.0000227

[52] N. Nadarajah, J.-A. Paffenholz, and P. J. G. Teunissen, "Integrated gnss attitude determination and positioning for direct geo-referencing," *Sensors*, vol. 14, no. 7, pp. 12 715–12 734, 2014. [Online]. Available: https://www.mdpi.com/1424-8220/14/7/12715

[53] D. Medina, "Robust GNSS Carrier Phase-based Position and Attitude Estimation," Ph.D. dissertation, Universidad Carlos III de Madrid, March 2022. [Online]. Available: https://elib.dlr.de/186624/

[54] D. Medina, A. Heßelbarth, R. Büscher, R. Ziebold, and J. García, "On the kalman filtering formulation for rtk joint positioning and attitude quaternion determination," in *2018 IEEE/ION Position, Location and Navigation Symposium (PLANS)*, 2018, pp. 597–604.

[55] T. D. Barfoot, *State estimation for robotics*. Cambridge University Press, 2017.

[56] J. Sola, J. Deray, and D. Atchuthan, "A micro lie theory for state estimation in robotics," *arXiv preprint arXiv:1812.01537*, 2018.

[57] S. I. Roumeliotis, G. S. Sukhatme, and G. A. Bekey, "Circumventing dynamic modeling: Evaluation of the error-state kalman filter applied to mobile robot localization," in *Proceedings 1999 IEEE International Conference on Robotics and Automation (Cat. No. 99CH36288C)*, vol. 2. IEEE, 1999, pp. 1656–1663.

[58] N. Trawny and S. I. Roumeliotis, "Indirect kalman filter for 3d attitude estimation," *University of Minnesota, Dept. of Comp. Sci. & Eng., Tech. Rep*, vol. 2, p. 2005, 2005.

[59] J. Sola, "Quaternion kinematics for the error-state kalman filter," *arXiv preprint arXiv:1711.02508*, 2017.

[60] J. Boehm, A. Niell, P. Tregoning, and H. Schuh, "Global mapping function (gmf): A new empirical mapping function based on numerical

weather model data," *Geophysical Research Letters*, vol. 33, no. 7, 2006. [Online]. Available: https://agupubs.onlinelibrary.wiley.com/doi/abs/10.1029/2005GL025546
[61] J. Subirana, J. Zornoza, M. Hernández-Pajares, E. S. Agency, and K. Fletcher, *GNSS Data Processing*, ser. ESA TM. ESA Communications, 2013, no. v. 1. [Online]. Available: https://gssc.esa.int/navipedia/GNSS_Book/ESA_GNSS-Book_TM-23_Vol_I.pdf
[62] J. Solà, "Quaternion kinematics for the error-state kalman filter," *CoRR*, vol. abs/1711.02508, 2017. [Online]. Available: http://arxiv.org/abs/1711.02508
[63] E.-H. Shin, "Estimation techniques for low-cost inertial navigation," Ph.D. dissertation, University of Calgary, May 2005. [Online]. Available: https://www.ucalgary.ca/engo_webdocs/NES/05.20219.EHShin.pdf
[64] Z. Gao, H. Zhang, M. Ge, X. Niu, W. Shen, J. Wickert, and H. Schuh, "Tightly coupled integration of multi-gnss ppp and mems inertial measurement unit data," *GPS Solutions*, vol. 21, no. 2, pp. 377–391, Apr 2017. [Online]. Available: https://doi.org/10.1007/s10291-016-0527-z
[65] D. Medina, J. Vilà-Valls, A. Hesselbarth, R. Ziebold, and J. García, "On the recursive joint position and attitude determination in multi-antenna gnss platforms," *Remote Sensing*, vol. 12, no. 12, 2020. [Online]. Available: https://www.mdpi.com/2072-4292/12/12/1955
[66] G. Welch and G. Bishop, "An introduction to the kalman filter," University of North Carolina at Chapel Hill, Chapel Hill, NC, USA, Tech. Rep. 95-041, 1995. [Online]. Available: http://www.cs.unc.edu/~welch/kalman/kalmanIntro.html
[67] T. Takasu, "Rtklib: open source program package for rtk-gps, foss4g 2009," *Tokyo: Free and Open Source Software for Geospatial (FOSS4G), Open Source Geospatial Foundation*, 2009. [Online]. Available: https://gpspp.sakura.ne.jp/paper2005/foss4g_2009_rtklib.pdf

VIII. Biography Section

Xiangdong An received his master and Ph.D. degrees in geodesy and survey engineering from GNSS Research Center of Wuhan University, Wuhan, China, in 2016 and 2020, respectively. He was a research fellow in the Institute of Communications and Navigation, German Aerospace Center (DLR) from 2020 to 2023. His is currently a research fellow at the School of Electrical and Electronic Engineering, Nanyang Technological University, Singapore. His research mainly focuses on real-time GNSS precise positioning and its integration with IMU.

Andrea Bellés received her B.S. in Aerospace Engineering from Universitat Politècnica de Catalunya (EETAC-UPC), Spain, and her M.S. in GNSS from the École Nationale de l'Aviation Civile (ENAC), University of Toulouse, France, in 2019 and 2021 respectively. Since 2022, she is a research fellow at the Institute of Communications and Navigation of the German Aerospace Center. Her research focuses on GNSS precise positioning in multi-antenna systems.

Filippo Giacomo Rizzi received his main degree in Communication and Computer Network Engineering in 2020 from Politecnico di Torino, Italy. He joined the German Aerospace Center (DLR) in 2020 where he works as a research scientist in the department of Nautical Systems of the Institute of Communications and Navigation. His research focuses on signal processing and receiver algorithm development for satellite and terrestrial positioning systems.

Lukas Hösch received his Diploma degree in Traffic and Transportation Engineering from Technische Universität Dresden in 2022. Right after this, he joined the department of Nautical Systems at the Institute of Communications and Navigation of the German Aerospace Center (DLR) as a research scientist. His activities include perception using cameras and LiDAR (light detection and ranging) sensors for HD-Mapping of inland waterways.

Christoph Lass earned his Ph.D. degree in mathematics from University of Greifswald in 2015. Since 2015 he works as a research fellow at the German Aerospace Center (DLR) in the Department of Nautical Systems of the Institute of Communications and Navigation, where he is part of the multi sensor systems group. His research interests include precise positioning in multi-antenna systems, noise analysis of GNSS signals and maritime integrity concepts.

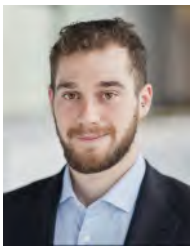

Daniel Medina (Member, IEEE) received the M.S. and Ph.D. degrees in Computer Sciences from Universidad Carlos III de Madrid (UC3M) in 2016 and 2022, respectively. He is currently a research fellow at the Institute of Communications and Navigation of the German Aerospace Center (DLR), where he leads the Multi Sensor Systems research group, dedicated to the provision of perception and navigation solutions for waterborne transport applications. His research interests include statistical signal processing at large, robust filtering and estimation theory with applications to LiDAR perception and high precision satellite-based navigation. He is currently the elected Vice-Chair for the IEEE ITSS German Chapter. He is actively involved in the editorial and organizational processes of a number of conferences, such as ITSC 2019–2023, IV 2022, IEEE/ION PLANS 2023 or the ITSS R8 Chapters Meeting 2023.